Automatic traveling wave excitation of structures with imperfect cyclic symmetry

Eyal Baruch[1, a], Yoav Vered[2], Harel Plat[1] and Izhak Bucher[1]

1 – Dynamics Laboratory, Faculty of Mechanical Engineering, Technion – Israel Institute of Technology, Haifa 3200003, Israel

2 – Institute of Sound and Vibration Research, University of Southampton, Southampton, SO17 1BJ, United Kingdom

Date: May 1, 2022

Keywords: Traveling waves; Ultrasonic motors; Autoresonance; Extremum seeking; Wave control

[a] Electronic mail: eyalbaruch@campus.technion.ac.il

Abstract

A method to generate traveling waves with maximal amplitudes in elastic structures with imperfect cyclic symmetric topology is presented. Traveling waves are useful in testing turbine-bladed disks and for the propulsion of ultrasonic motors. However, open-loop excitation of traveling waves may yield a partially standing wave due to imperfections and mode-mistuning. The present work puts forward a method that automatically locks onto the optimal excitation of the system, producing the largest possible pure propagating wave. The excitation uses autoresonance with modal filtering, and force projection control, utilizing optimum-seeking methodology. To validate the presented method, an experimental system consisting of a ring of coupled acoustic Helmholtz resonators was built. The ring was excited by the proposed method, and the ability to overcome the imperfections and automatically lock onto the optimal excitation was observed. In addition, the method was realized on a simulated, ultrasonic, acoustic levitation motor that utilizes traveling waves to control levitated objects.

1. Introduction

Traveling wave excitation is used in various dynamical systems, such as ultrasonic motors (USMs) [1], acoustic levitational motors [2], impedance tubes [3], thermoacoustic electric generators [4] antennas [5], bladed disks [6] and even clock generators [7]. In such instances, it is vital to control the nature of the traveling wave to obtain maximal efficiency. Therefore, traveling wave propagation was examined in several different cases. Chow et al. [8] investigated the stability of traveling waves in lattice systems. The propagation of traveling waves in flexible rotating rings was discussed in [9], comparing experimentally obtained natural frequencies to analytical findings. An analysis of resonant traveling waves in rotating rings was presented in [10], including the effects of nonlinear dynamics. Parametric excitation is employed in [11] to create multi-wavelength traveling waves in a ring.

Systems with cyclic symmetry are fit for the excitation of traveling waves since they experience doublet modes that allow the propagation of such waves at resonance [12]. As a result, different approaches were taken to exploit this phenomenon in cyclic symmetric actuators. PID controllers can be used to precisely control the speed of rotation of USMs. For example, see reference [13], where a PID was designed to lock onto the desired rotation speed based on a measured model of the motor and two expert rules. In addition, to overcome performance problems due to dead zone dynamics, which are common in USMs, [14] proposed a nonlinear model of a USM that includes dead-zone dynamics and proposed a controller which dictates both the phase difference and velocity of the motor. An iterative PID controller tuning method was implemented in [15] to overcome unknown nonlinearities in the system. Finally, the effect of the excitation amplitude, phase, and frequency on the speed of rotation of a USM is examined in [16], where a phase-locked loop controller was implemented to track the resonance frequency of the motor.

An important factor of USMs is the motor's efficiency [47]. It was previously optimized by modifying the stator geometry [17] or by choosing the excitation frequency to maximize the contributing energy of a USM model [18]. The efficiency of a USM at different frequencies, phase differences, and duty cycles was measured in [19]. In addition, [20], presented a method for tracking the parallel resonance of USMs, which changes over time.

However, all of these approaches rely on a perfectly cyclic-symmetric system model. They do not consider the option of mode splitting caused by geometric and material imperfections that break the cyclic symmetry [21]. The imperfections create a frequency split that affects the system's dynamic behavior and may prevent the generation of pure, uniform amplitude traveling waves [22]. These issues give rise to higher local amplitudes, which are inefficient and unwanted. It has been shown that these effects are not negligible

in USMs [23]. As a result, reference [23] proposed to optimize the geometry of the USM teeth. However, this method does not consider other factors that cause a frequency split, such as manufacture tolerances, temperature differences, or non-symmetrical loading.

The following paper aims to overcome this problem using phase and amplitude optimization combined with frequency control. In addition, the presented method uses adaptive control to handle changes in the system's dynamics over time.

To assist in optimizing and quantifying the traveling wave purity, the traveling wave ratio (TWR), defined in [24], is used. For a ring-like structure, a distributed, monochromatic vibration pattern along the circumference can be represented as the sum of two waves traveling in opposite directions

$$w(\theta,t)=\Re\left(U_{+}e^{i(\omega t-\kappa\theta)}+U_{-}e^{i(\omega t+\kappa\theta)}\right), \tag{1}$$

where U_{+} and U_{-} are the amplitudes of the forward and backward propagating waves along the circumference, θ. Also, κ denotes the circumferential wavelength and ω the frequency of vibration.

One can define the TWR as:

$$\mathrm{TWR}=1-\left|\frac{|U_{+}|-|U_{-}|}{|U_{+}|+|U_{-}|}\right|. \tag{2}$$

The TWR is a scalar ranging between 0 and 1. For TWR=1, a pure standing wave is obtained, while for TWR=0, a pure traveling wave takes place. Therefore, the TWR is a suitable candidate to serve as a cost function when optimizing the vibratory response of the system, since it is bounded and reaches the optimal result at its extremum (TWR=0).

The excitation of traveling waves necessitates multiple actuators operating at an optimal frequency whose spatial location and relative phase are optimally set. A candidate method for tuning these parameters is the extremum seeking approach, which is a gradient-descent based method realizing an adaptive control loop [25]. This method is used in different applications, such as power optimization in photovoltaic systems [26] and PID controller tuning [27]. In the present work, extremum seeking is adapted to automatically tune various excitation-related parameters so that the vibratory response attains the optimal TWR.

The applied excitation should operate near resonance to achieve sufficiently large vibration amplitudes of the desired traveling waves. Autoresonance (AR) is a nonlinear relay-based feedback control method used to excite linear systems at resonance [28,29], employing a phase-shifted measured response. This method tracks the resonance frequency in the presence of slow changes and is used in atomic force microscopes to measure nano-scale topology details [30]. Reference [31] introduced a phase shifter to control the modal regime of a nonlinear dynamic system oscillation. Phase control can be used to optimize the amplitude of

oscillations since the frequency that the AR locks on depends on the relative phase lag of the response signal and the excitation [32]. The modal filtered AR feedback [33] can be used to excite a single desirable mode in multi-degrees of freedom (MDOF) systems. Reference [34] used the modal filtered AR (MFAR) to develop an acoustic levitation based motor by creating a traveling wave in an annulus. In these works, it was assumed that the cyclic imperfection is small, and consequently, a suboptimal result was obtained. In this research, a traveling wave autoresonance (TWAR) control loop is designed to propagate optimal traveling waves near resonance.

The method presented in this paper is validated experimentally on an acoustic cyclic symmetric system consisting of a ring of Helmholtz resonators (HR) with connected necks. The ring is modeled as a chain of masses and springs emanating from an extended lumped model of a single HR [35][36]. The resonators are excited by loudspeakers, and microphones measure their internal pressure. Extremum seeking is used to optimize the excitation parameters.

The paper is outlined as follows: Section 2 presents the dynamics of the imperfect, cyclically symmetric lumped model used to describe the system. Section 3 introduces the form of excitation that will ensure the propagation of traveling waves. Section 4 explores the effect of the proposed form of excitation on the amplitude of the traveling waves. Section 5 demonstrates the application of the method on an ultrasonic motor exploiting traveling waves using finite element simulations. Finally, section 6 presents experimental results on the acoustic experimental system, examining the performance of the proposed method.

2. System dynamics

For the development of a method producing pure traveling waves, a model of a cyclic symmetric system, presented in Figure 1, is considered. The dynamic behavior of this system is expressed both using its mode shapes and in terms of the propagation of forward and backward traveling waves.

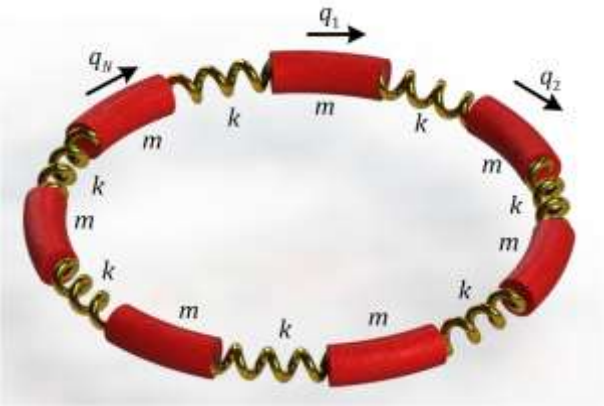

Figure 1 – A lumped parameter model of a cyclic system consisting of a masses and springs chain. The damping in the system is assumed to be both modal and weak and will be denoted using ζ. Consequently, the eigenvectors remain real and are not coupled by damping forces.

The actuation scheme for these systems can vary depending on the application and the realization. For instance, USMs utilize 2 excitation inputs that are in 90 degrees phase. These inputs actuate 2 distributed electrodes, each exciting a single mode [16]. Conversely, the acoustic levitation ring discussed later has 3 points of excitation that are situated 120 degrees apart, which is suitable (see [2]) for the n=11 nodal diameter modes being controlled. Therefore, appropriate phasing in time is chosen for each of the 3 actuators, as explained in [2]. In both cases, the relative phases and amplitudes can be chosen to accommodate frequency split and deviation from perfect cyclic symmetry. In the following section, a general actuation method will be proposed, which refers to each degree of freedom in the system and can be applied to any system with multiple actuation inputs.

2.1 Mode shapes of perfect cyclic symmetric systems

For the system presented in Figure 1, which is perfectly cyclically symmetric, the linear equations of motion result in the following mass and stiffness matrices:

$$M_0 = \begin{bmatrix} 1 & & \\ & \ddots & \\ & & 1 \end{bmatrix} m, \quad K_0 = \begin{bmatrix} 2 & -1 & 0 & \cdots & 0 & -1 \\ -1 & 2 & \ddots & & & 0 \\ 0 & \ddots & \ddots & \ddots & & \vdots \\ \vdots & & \ddots & \ddots & \ddots & 0 \\ 0 & & & \ddots & \ddots & -1 \\ -1 & 0 & \cdots & \cdots & -1 & 2 \end{bmatrix} k, \quad \in \mathbb{R}^{N \times N}, \tag{3}$$

where m and k denote the identical mass and spring elements. Considering the steady-state response of this system to a vector of monochromatic sinusoidal forces with amplitudes $\mathbf{F}$, the response vector, $\mathbf{q}$, can be found by solving [37]

$$\left(K_0 - \omega^2 M_0\right)\mathbf{q} = \mathbf{F}, \quad \mathbf{q} \triangleq \begin{pmatrix} q_1 & q_2 & \cdots & q_N \end{pmatrix}^T, \mathbf{F} \triangleq \begin{pmatrix} F_1 & F_2 & \cdots & F_N \end{pmatrix}^T, \tag{4}$$

where the coordinates are denoted as $q_1 \ldots q_N$, as shown in Figure 1, and ω is the frequency of excitation. Circular systems composed of identical segments (as discussed in this example) give rise to doublet modes [38], which share the same natural frequency. These doublet modes solve the eigenvalue problem:

$$\left(K_0 - \omega_n^2 M_0\right)\boldsymbol{\phi}_n = 0, \quad n = 1 \ldots N, \tag{5}$$

where ω_n^2 is the eigenvalue corresponding to the eigenvectors $\boldsymbol{\phi}_n$, $\boldsymbol{\phi}_{n+1}$. The two associated eigenvectors can be expressed as a function of their angular location [12,39,40]:

$$\phi_{2p-1,s} = \sin\left(2\pi ps / N\right), \quad \phi_{2p,s} = \cos\left(2\pi ps / N\right), \tag{6}$$

where N denotes the number of degrees of freedom (DOF), $p = 0, \cdots, \lfloor N/2 \rfloor$ is the wavenumber, and $s = 1, \cdots, N$ is the coordinate number. Since, for perfectly circular systems, both mode shapes have the same natural frequency, any linear combination satisfies the same generalized eigenvalue problem:

$$\left(K_0 - \omega_n^2 M_0\right)\left(A\boldsymbol{\phi}_n + B\boldsymbol{\phi}_{n+1}\right) = 0. \tag{7}$$

Equation (7) demonstrates that the eigenvector corresponding to ω_n^2 has a non-unique spatial distribution and therefore both standing, traveling waves and their combination are possible solutions. When some small imperfection exists in the system, the mode shapes in Eq. (6) are no longer arbitrary, and their spatial arrangement is fixed. Furthermore, the doublet mode is split, and their respective natural frequencies are no longer identical [41], although close.

3. Excitation of traveling waves

To excite traveling waves in a cyclic symmetric system at resonance, the doublet mode shapes presented in Eq. (6) must be excited in a 90 degrees phase in time. However, due to deviations from cyclic symmetry, the modes and natural frequencies of the system change. The mode shapes can be approximated by assuming, similar to the assumption used in [42], that the imperfections are small, leading to:

$$\begin{aligned} \boldsymbol{\phi}_1 &\approx \cos\left(2\pi \mathbf{s} / N + \varphi_0\right) \\ \boldsymbol{\phi}_2 &\approx \sin\left(2\pi \mathbf{s} / N + \varphi_0\right) \end{aligned}, \tag{8}$$

where the phase φ_0 is no longer arbitrary. By performing a shift in the coordinates $\tilde{\boldsymbol{q}} = \boldsymbol{q} - \frac{N\varphi_0}{\pi}$, the mode shapes take the following form:

$$\begin{aligned} \boldsymbol{\phi}_1 &\approx \cos\left(2\pi \mathbf{s}/N\right) \\ \boldsymbol{\phi}_2 &\approx \sin\left(2\pi \mathbf{s}/N\right) \end{aligned}. \tag{9}$$

Assuming modal damping ζ_n, the frequency n^{th} frequency response is:

$$H_n(\omega) \triangleq \frac{\eta_n}{Q_n} = \frac{1}{\omega_n^2 - \omega^2 + \mathrm{i}2\zeta_n\omega\omega_n}, \qquad n = 2p-1, 2p\,. \tag{10}$$

where η_n is the amplitude of the n^{th} mode, and Q_n denotes the projection of the excitation force onto the n^{th} mode. Assuming the excitation force frequency is close to the natural frequency ω_n, it is possible to neglect the influence of higher doublet modes due to the strong attenuation when far from the natural frequency. Therefore, the response of the system to a forced excitation **F** will be [43] :

$$\mathbf{q}(\omega) = \frac{1}{\tilde{m}}\left(H_1(\omega)\boldsymbol{\phi}_1\boldsymbol{\phi}_1^T\mathbf{F} + H_2(\omega)\boldsymbol{\phi}_2\boldsymbol{\phi}_2^T\mathbf{F}\right), \tag{11}$$

Where $\tilde{m}$ is the assumed uniform modal mass. Due to mode split [44], $H_1(\omega)$ and $H_2(\omega)$ have different complex amplitudes. As a result, choosing a form of excitation **F** with uniform amplitude and phase projection on both modes gives rise to a partially traveling and partially standing wave. Amplitude and phase control is introduced to propagate a pure traveling wave, resulting in excitation force of the following form:

$$\mathbf{F} = \left(\cos(\theta)\cos(\varphi + \kappa\mathbf{s}) - i\sin(\theta)\sin(\varphi + \kappa\mathbf{s})\right)4e^{i\omega t} + cc\,, \tag{12}$$

where θ and φ are the controlled parameters determining the amplitude and phase of the excitation of each mode, and $\kappa = 2\pi/N$. Here *cc* stands for the complex conjugate of the first term. In the case of only 2 excitation forces, the phase φ can be replaced by a time phase to achieve similar results (see appendix A). The projection of the excitation on the mode shapes, constituting the modal forces [25], is:

$$\begin{bmatrix} \boldsymbol{\phi}_1^T\mathbf{F} \\ \boldsymbol{\phi}_2^T\mathbf{F} \end{bmatrix} = \|\boldsymbol{\phi}\|^2 \begin{bmatrix} \cos(\theta)\left(\cos(\varphi)\right) - i\sin(\theta)\left(\sin(\varphi)\right) \\ \cos(\theta)\left(-\sin(\varphi)\right) - i\sin(\theta)\left(\cos(\varphi)\right) \end{bmatrix} 4e^{i\omega t} + cc\,, \tag{13}$$

where the mode shapes are scaled as $||\boldsymbol{\phi}||^2 = \boldsymbol{\phi}_1^T\boldsymbol{\phi}_1 = \boldsymbol{\phi}_2^T\boldsymbol{\phi}_2$.

By denoting $H_1 = |H_1|e^{i\alpha_1}, H_2 = |H_2|e^{i\alpha_2}$, and normalizing the modal norm, the steady-state response of the system will be:

$$\mathbf{q}(\omega)=\begin{pmatrix}\boldsymbol{\phi}_1\begin{pmatrix}\left(|H_1|C_{\alpha_1}C_\theta C_\varphi+|H_1|S_{\alpha_1}S_\theta S_\varphi\right)\cos(\omega t)\\+\left(|H_1|C_{\alpha_1}S_\theta S_\varphi-|H_1|S_{\alpha_1}C_\theta C_\varphi\right)\sin(\omega t)\end{pmatrix}+\\\boldsymbol{\phi}_2\begin{pmatrix}\left(-|H_2|C_{\alpha_2}C_\theta S_\varphi+|H_2|S_{\alpha_2}S_\theta C_\varphi\right)\cos(\omega t)\\+\left(|H_2|C_{\alpha_2}S_\theta C_\varphi+|H_2|S_{\alpha_2}C_\theta S_\varphi\right)\sin(\omega t)\end{pmatrix}\end{pmatrix}, \tag{14}$$

where $C_* = \cos(*)$, $S_* = \sin(*)$. An abbreviation for Eq. (14) is:

$$\mathbf{q}=\left(a_1\boldsymbol{\phi}_1+a_2\boldsymbol{\phi}_2\right)\cos(\omega t)+\left(b_1\boldsymbol{\phi}_1+b_2\boldsymbol{\phi}_2\right)\sin(\omega t), \tag{15}$$

where

$$\begin{aligned}a_1&=|H_1|C_{\alpha_1}C_\theta C_\varphi+|H_1|S_{\alpha_1}S_\theta S_\varphi\\a_2&=-|H_2|C_{\alpha_2}C_\theta S_\varphi+|H_2|S_{\alpha_2}S_\theta C_\varphi\\b_1&=|H_1|C_{\alpha_1}S_\theta S_\varphi-|H_1|S_{\alpha_1}C_\theta C_\varphi\\b_2&=|H_2|C_{\alpha_2}S_\theta C_\varphi+|H_2|S_{\alpha_2}C_\theta S_\varphi\end{aligned}. \tag{16}$$

By using the complex notation employing Euler's formula, the amplitudes of the forward and backward propagating waves introduced in Eq. (1) are (see [34,45]):

$$U_+=\sqrt{\left(a_1+b_2\right)^2+\left(a_2-b_1\right)^2},U_-=\sqrt{\left(a_1-b_2\right)^2+\left(a_2+b_1\right)^2}. \tag{17}$$

For a pure traveling wave to propagate in the system, either U_+ or U_- must vanish.

U_+ vanishes when $|a_1 + b_2| = |a_2 - b_1| = 0$, resulting in:

$$\begin{aligned}&|H_1|C_{\alpha_1}C_\theta C_\varphi+|H_1|S_{\alpha_1}S_\theta S_\varphi+|H_2|C_{\alpha_2}S_\theta C_\varphi+|H_2|S_{\alpha_2}C_\theta S_\varphi=0\\&-|H_2|C_{\alpha_2}C_\theta S_\varphi+|H_2|S_{\alpha_2}S_\theta C_\varphi-|H_1|C_{\alpha_1}S_\theta S_\varphi+|H_1|S_{\alpha_1}C_\theta C_\varphi=0\end{aligned}, \tag{18}$$

Note that for the special case of a symmetric system ($|H_1| = |H_2|, \alpha_1 = \alpha_2$), Eq. (18) becomes:

$$\begin{aligned}&\left(C_\alpha C_\varphi+S_\alpha S_\varphi\right)\left(C_\theta+S_\theta\right)=0\\&\left(-C_\alpha S_\varphi+S_\alpha C_\varphi\right)\left(C_\theta+S_\theta\right)=0\end{aligned}. \tag{19}$$

From this set of equations, it is evident that for $C_\theta = -S_\theta$ Eq. (19) upholds regardless of φ. This is expected, as in a fully symmetric system the phase of excitation does not affect the response. For an imperfect system, rearranging Eq. (18):

$$T_\varphi=-\frac{|H_1|C_{\alpha_1}C_\theta+|H_2|C_{\alpha_2}S_\theta}{|H_1|S_{\alpha_1}S_\theta+|H_2|S_{\alpha_2}C_\theta}=\frac{|H_2|S_{\alpha_2}S_\theta+|H_1|S_{\alpha_1}C_\theta}{|H_2|C_{\alpha_2}C_\theta+|H_1|C_{\alpha_1}S_\theta}, \tag{20}$$

where $T_\varphi = \tan(\varphi)$. Applying trigonometric identities:

$$S_{2\theta} = -\frac{2|H_1||H_2|}{|H_1|^2 + |H_2|^2} C_{\alpha_1-\alpha_2}. \tag{21}$$

In the region of $[0, \pi]$, the solution for Eq. (21) is:

$$\theta = \arcsin\left(-\frac{|H_1||H_2|}{|H_1|^2 + |H_2|^2} C_{\alpha_1-\alpha_2} \right).. \tag{22}$$

The value of φ can be derived similarly:

$$T_{2\varphi} = \frac{2|H_1||H_2|}{|H_1|^2 - |H_2|^2} S_{\alpha_2-\alpha_1}, \tag{23}$$

resulting in 2 solutions for φ in the region of $[0, \pi]$, of:

$$\varphi_1 = \arctan\left(\frac{|H_1||H_2|}{|H_1|^2 - |H_2|^2} S_{\alpha_2-\alpha_1} \right), \varphi_2 = \arctan\left(\frac{|H_1||H_2|}{|H_1|^2 - |H_2|^2} S_{\alpha_2-\alpha_1} \right) + \pi/2. \tag{24}$$

In the same manner, it is possible to find two additional combinations for $U_- = 0$.

From these findings, it is evident that four combinations of φ and θ that produce pure traveling waves exist. To understand if there is a preferred combination of φ and θ, it is of interest to evaluate the amplitude of the traveling wave in each combination. For the sake of brevity, the damping in the system is omitted, resulting in

$$H_n = \frac{1}{\omega_n^2 - \omega^2} \triangleq \frac{1}{\Delta_n}. \tag{25}$$

$\omega_n^2 \neq \omega^2$ must hold to ensure participation of both modes. The amplitudes of the forward and backward propagating waves are

$$U_+ = \frac{4\|\boldsymbol{\phi}\|^2}{\Delta_1\Delta_2} \sqrt{\left(\Delta_2 C_\theta C_\varphi + \Delta_1 S_\theta C_\varphi\right)^2 + \left(\Delta_1 C_\theta S_\varphi - \Delta_2 S_\theta S_\varphi\right)^2}, \tag{26}$$

$$U_- = \frac{4\|\boldsymbol{\phi}\|^2}{\Delta_1\Delta_2} \sqrt{\left(\Delta_2 C_\theta C_\varphi - \Delta_1 S_\theta C_\varphi\right)^2 + \left(\Delta_1 C_\theta S_\varphi + \Delta_2 S_\theta S_\varphi\right)^2}. \tag{27}$$

The four possible combinations of φ and θ are:

$$(\varphi,\theta)_{1,3} = \left(\frac{\pi}{2}, \pm\tan^{-1}\left(\frac{\Delta_1}{\Delta_2}\right) \right), (\varphi,\theta)_{2,4} = \left(0, \mp\tan^{-1}\left(\frac{\Delta_2}{\Delta_1}\right) \right). \tag{28}$$

Plugging Eq. (28) into Eq.(26), (27), consequently, result in the amplitude of the traveling wave as:

$$U_1 = U_2 = U_3 = U_4 = \frac{8\|\boldsymbol{\phi}\|^2}{\sqrt{\Delta_1^2 + \Delta_2^2}}, \tag{29}$$

Since the amplitudes of the different combinations are uniform, there is no preferred combination. Clearly, in the presence of damping, slightly different values for the amplitudes are expected, but a slight adjustment of the governing phases is expected to remedy these changes.

In order to find the parameters θ and φ, which will result in a pure traveling wave, a filter that provides an online approximation of the TWR was designed. The TWR is then used as a cost function for the extremum seeking procedure, which perturbs θ and φ to find their optimal values. The excitation's frequency, ω, is being determined via traveling wave AR (TWAR), with modal filtering and amplitude control that depends on θ and φ. A flowchart of the entire process is presented in Figure 2.

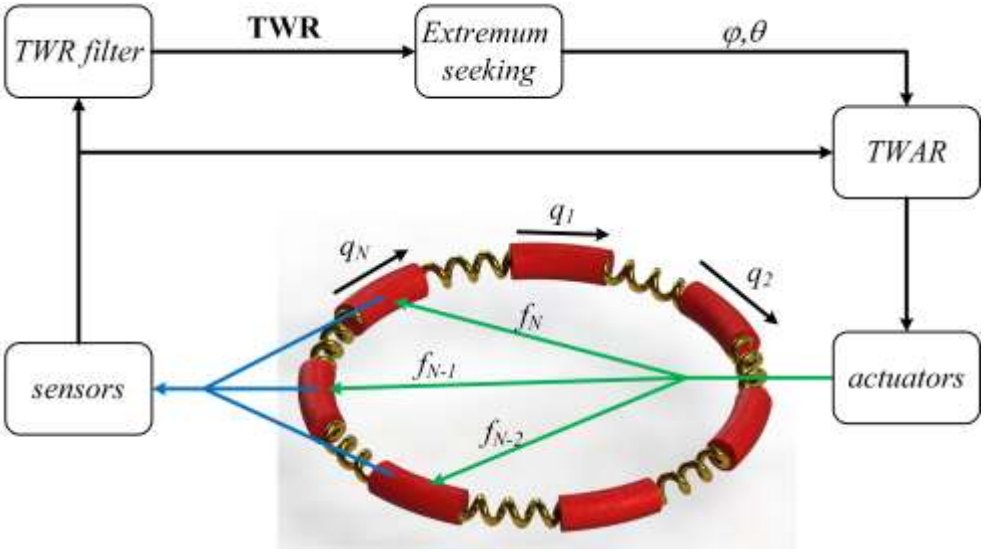

Figure 2 – A flowchart of the traveling wave automatic tuning method. The TWR filter (Figure 3) approximates the TWR using the measured displacements. The extremum seeking (Figure 5) employed the TWR to find the optimal values of θ and φ. Then, The TWAR loop (Figure 6) excites the system in a traveling wave at resonance.

The TWR filter extracts the information about the ratio of traveling to standing waves using several circumferentially deployed sensors along the structure. The TWR filter will be presented in section 3.1 together with the extremum seeking control method in 3.2. Finally, the TWAR, which generates the AR excitation driving the circumferentially deployed actuators, will be shown in 3.3.

3.1 Real-time calculation of the TWR

An estimation method of the response's TWR is derived for the optimization of θ and φ, required for the TWR minimization. While other methods like calculating the power flow in the system [46] exist, the method presented here is preferred. The advantages of the described method are its ability to employ real-time filtering and handle multiple sensors.

It is assumed that the response of a system to a single excitation frequency, ω, can be described as the superposition of a forward and backward traveling wave, as presented in Eq. (1). To approximate the TWR, the amplitudes U_+ and U_- must be approximated. To this end, one may observe that the squared norm of the system response, $\mathbf{q}$, is of the form:

$$\mathbf{q}^T\mathbf{q} = U_+^2\|\boldsymbol{\phi}\|^2 + U_-^2\|\boldsymbol{\phi}\|^2 + 2U_+U_-\|\boldsymbol{\phi}\|^2\cos(2\omega t). \tag{30}$$

Using a low pass filter (LPF), the scalar signal can be divided into two parts:

$$\begin{aligned} S_1 &= \|\boldsymbol{\phi}\|^2\left(U_+^2 + U_-^2\right) \\ S_2 &= \|\boldsymbol{\phi}\|^2 2U_+U_-\cos(2\omega t) \end{aligned} \tag{31}$$

A low pass of S_2^2 is then calculated:

$$LPF\left(S_2^2\right) = LPF\left(\left(2\|\boldsymbol{\phi}\|^2U_+U_-\right)^2\left(\frac{1}{2}\left(1+\cos(4\omega t)\right)\right)\right) = \frac{1}{2}\left(2\|\boldsymbol{\phi}\|^2U_+U_-\right)^2 \tag{32}$$

Multiplying by 2 and taking the square root of the result:

$$\tilde{S}_2 = 2\|\boldsymbol{\phi}\|^2U_+U_- \tag{33}$$

By using algebraic manipulation and substituting into Eq. (2), it is possible to calculate the TWR as:

$$TWR = 1 - \frac{\sqrt{S_1 - \tilde{S}_2}}{\sqrt{S_1 + \tilde{S}_2}} \tag{34}$$

A flowchart of the proposed real-time TWR filter is presented in Figure 3:

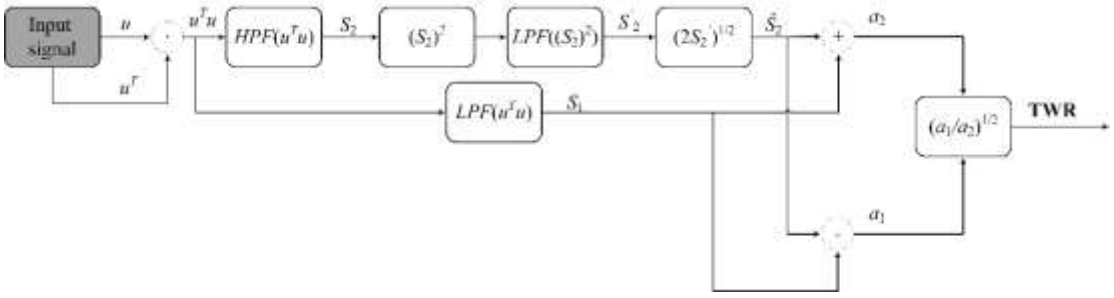

Figure 3 – Flowchart of the filter for real-time calculation of the TWR in the block diagram of Figure 5.

In conclusion, the presented filter allows the real-time approximation of the TWR. Since the filter can be implemented on a digital controller, the TWR can be used as a parameter for real-time optimization, as proposed.

3.2 Extremum seeking

To find φ and θ optimal values, extremum seeking [25] adaptive control is introduced to the proposed excitation method. Adaptive control of φ and θ will allow the finding and tracking of the optimal parameters if the system's dynamics vary. The performance function to be minimized in the control loop is the TWR, as defined in Eq. (2), which is estimated in real-time based on the filter of Section 3.1. The optimized parameters are θ, which controls the amplitude of the modal excitation, and φ, which controls the phase. Since the TWR is bounded between [0,1], and the parameters θ and φ are periodic, the cost function must obtain a global minimum within the defined domain. A schematic diagram of the control loop is presented in Figure 4:

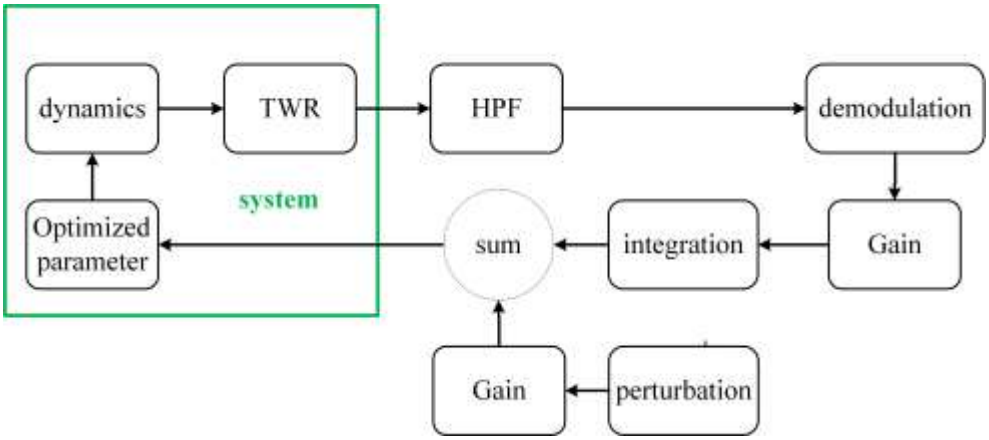

Figure 4 – The block diagram of the extremum seeking loop. A gradient descent adaptive law is implemented using the perturbation, high-pass-filter (HPF), demodulation, and integration. The optimized parameter converges to steady state when the cost function is at extremum.

The parameter to be optimized is perturbed sinusoidally, and the perturbation's time constant is chosen to be an order of magnitude slower than that of the system. Gradient descent optimization is performed by applying a high pass filter (HPF), demodulation, and integration filters on the cost function's output. The amplitude of the filtered signal gain controls the step size of the gradient descent, and the sign determines whether optimization will seek minimum or maximum. A proof of the steady-state convergence of the control loop arriving at the extremum is presented in [25]. This method can be applied to multiple parameters by varying the frequency of perturbations, as claimed in [25] and shown in the following section.

3.2.1 Extremum seeking for multiple parameters

Using the proposed form of excitation, the TWR is a function of the two parameters φ and θ. By assuming that the variables φ and θ are independent, TWR can be expressed as

$$TWR = TWR(\theta, \varphi). \tag{35}$$

By perturbing both parameters in different frequencies

$$\theta = \theta_0 + \theta_1 \cos(\Omega_1 t), \varphi = \varphi_0 + \varphi_1 \cos(\Omega_2 t), \theta_1 \ll \theta_0, \varphi_1 \ll \varphi_0, \tag{36}$$

and using Taylor expansion, the TWR can be approximated as:

$$TWR = TWR_0 + \frac{\partial TWR}{\partial \theta}\theta_1 \cos(\Omega_1 t) + \frac{\partial TWR}{\partial \varphi}\varphi_1 \cos(\Omega_2 t) + H.O.T. \tag{37}$$

By applying the HPF and demodulating the signal with $\cos(\Omega_1)$, the signal becomes:

$$s = \frac{\partial TWR}{\partial \theta}\theta_1 \frac{1}{2}\left(1 + \cos(2\Omega_1 t)\right) + \frac{\partial TWR}{\partial \varphi}\varphi_1 \frac{1}{2}\left(\cos\left((\Omega_2 + \Omega_1)t\right) + \cos\left((\Omega_2 - \Omega_1)t\right)\right). \tag{38}$$

Note that the signal *s* is oscillating. Denoting:

$$\Omega_2 = \Omega_1 + \Delta\Omega. \tag{39}$$

Eq. (38) becomes:

$$s = \frac{\partial TWR}{\partial \theta}\theta_1 \frac{1}{2}\left(1 + \cos(2\Omega_1 t)\right) + \frac{\partial TWR}{\partial \varphi}\varphi_1 \frac{1}{2}\left(\cos\left((2\Omega_1 + \Delta\Omega)t\right) + \cos\left((\Delta\Omega)t\right)\right). \tag{40}$$

Since

$$\int_0^{\frac{2\pi n}{\tilde{\Omega}}} \cos(\tilde{\Omega} t)dt = 0 \tag{41}$$

for any parameter $\tilde{\Omega}$, and in addition, it is possible to choose Ω_2, Ω_1 so there exists n_1, n_2, n_3 for which

$$T = \frac{2\pi n_1}{2\Omega_1} = \frac{2\pi n_2}{2\Omega_1 + \Delta\Omega} = \frac{2\pi n_3}{\Delta\Omega}. \tag{42}$$

The integration of *s* over T will cancel the oscillating components, remaining with

$$\theta = \int_0^{nT} \frac{\partial TWR}{\partial \theta}\frac{\theta_1}{2}dt' = \theta_{n-1} + \frac{\pi\theta_1 n_1}{\Omega_1}\frac{\partial TWR}{\partial \theta}, \tag{43}$$

where θ_{n-1} is the integration for the first $n-1$ cycles of *T*. Therefore, integration of the filtered and demodulated cost function is equivalent to a gradient descent optimization in the direction where a change in θ reduces the TWR. It is worth noting that for larger values of $\Delta\Omega$ the time constant *T* will be smaller,

resulting in faster convergence. Similarly, a signal proportional to the partial derivative with respect to φ can be obtained. While this adaptive control method enables the finding and tracking of the optimal parameters θ and φ, it also introduces a constant perturbation of these parameters, which reduces the effectiveness of the excitation. This problem can be improved by introducing a form of weighting to the perturbations resulting in lower modulations at the steady-state.

Since, at optimum, the TWR is 0, it is natural to use the TWR as a weighting of the amplitude of perturbations so that when the system reaches the optimal state of TWR=0, the parameters θ and φ will remain constant. Therefore, the perturbations are multiplied by an averaged TWR, resulting in minimal perturbations when TWR approaches 0. This does not harm the adaptive control, since if the system changes, the TWR will be greater than 0, allowing the optimization to come into effect. A block diagram of the control loop is presented in Figure 5.

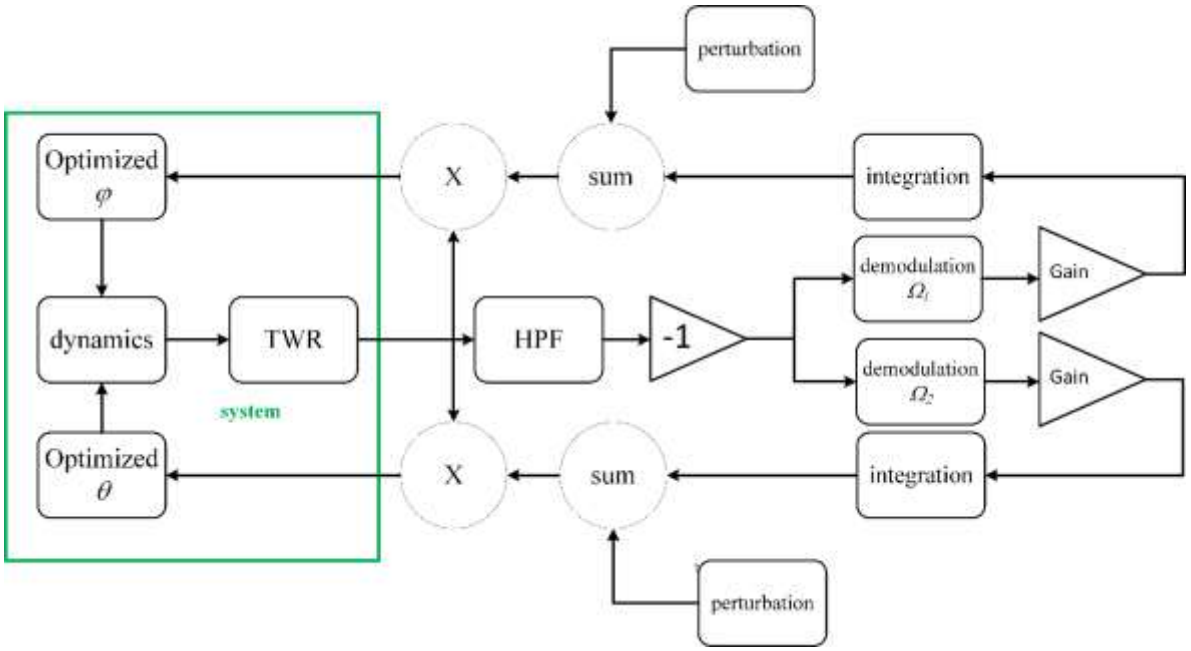

Figure 5 – Extremum seeking for two parameters θ and φ, with gain control using the TWR. θ controls the amplitude of the modal excitation, and φ controls the phase. The TWR is obtained from the filter previously presented in section 3.1.

3.3 Autoresonance excitation

For the excitation to have a maximal projection on a single wavelength, it is desirable to excite the system at resonance. This will be executed using an AR feedback loop designed to propagate traveling waves at resonance. AR is a nonlinear feedback loop designed to excite dynamic systems at their resonance frequencies automatically. The response of a SDOF system to AR excitation is presented in appendix B.

In this paper, a form of AR designed for traveling wave excitation is devised. A block diagram of the AR excitation is presented in Figure 6:

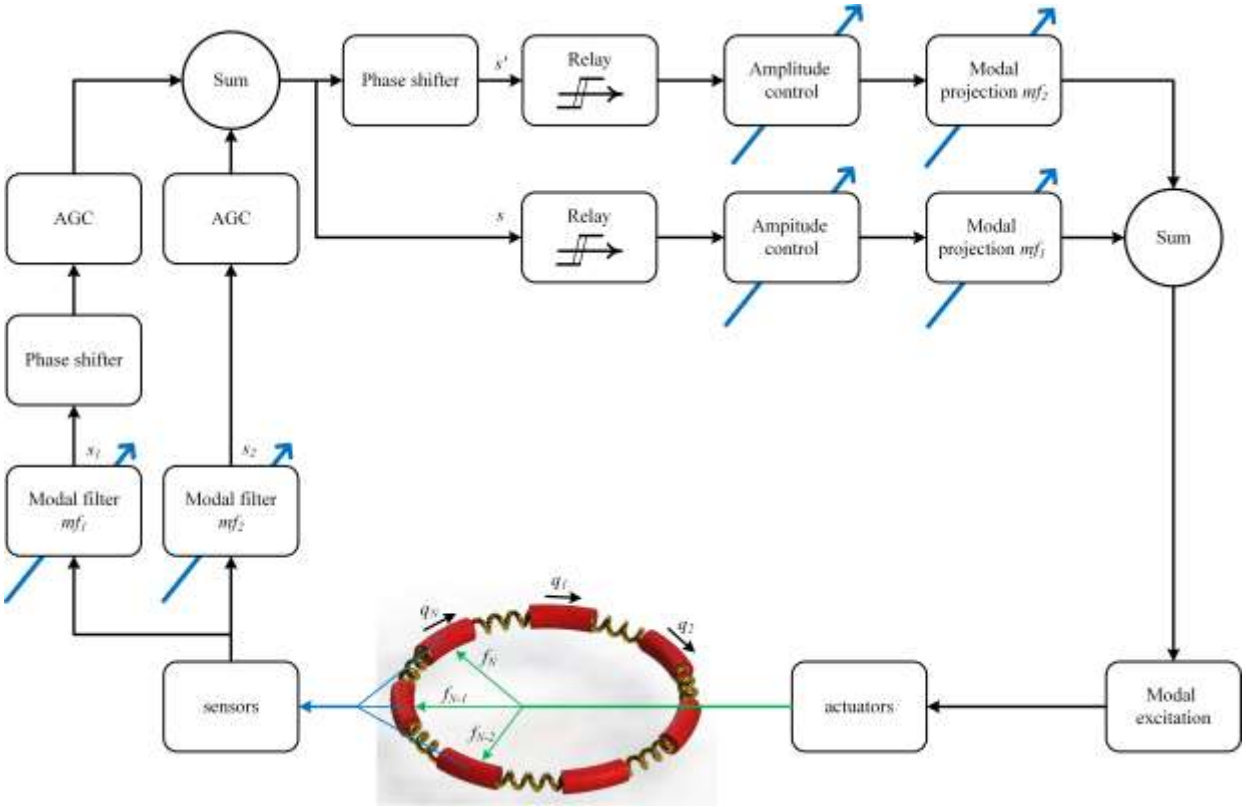

Figure 6 – The block diagram of the control loop that propagates traveling waves using AR with modal filtering. The modal filter blocks extract the projection of the system's response on the sine and cosine modes with a controllable phase. The phase shifter shifts the phase of one of the projections to 90 degrees (using differentiation), and the AGC blocks ensure uniform amplitudes of both signals. The relay acts as a sign function, and the modal projection blocks project the signal on the same spatial distribution as that of the modal filters. The resulting distributed signal excites the system via actuators.

As presented in Eq. (8), the mode shapes have sine and cosine spatial distribution with some initial phase. The response of the system **q** is a projected spatial sine, and a time phase-shifted spatial cosine. The two projections are summed, resulting in the projection of **q** on the traveling wave. Then, a phased shifted copy of the projection is obtained. Both the projection and its phase-shifted copy are passed through a relay. The original is projected on a spatial cosine wave, and the shifted one is projected on a sine. The control of the phase shift determines the amplitude of the temporal sine and cosine. Finally, the two signals are summed, and the system is excited with the resulting signal. The steady-state response of the system can be analyzed using the following steps:

For the control loop to actuate the system with a force as proposed in Eq. (12), the modal filters take the following form:

$$\begin{aligned} mf_1 &= \boldsymbol{\phi}_1 \sin(\varphi) + \boldsymbol{\phi}_2 \cos(\varphi), \\ mf_2 &= \boldsymbol{\phi}_1 \cos(\varphi) - \boldsymbol{\phi}_2 \sin(\varphi) \end{aligned} \tag{44}$$

and the amplitude control blocks are of the form:

$$G_1 = \cos(\theta), G_2 = \sin(\theta). \tag{45}$$

Both φ and θ are dictated by the extremum seeking control loop. Assuming there exists a steady-state single frequency response of the system, the signal s from the first summation will be:

$$s = A\cos(\omega t), \tag{46}$$

for unknowns A and ω. Choosing the phase shifter to be a derivative, the signal s' becomes:

$$s' = -A\omega \sin(\omega t). \tag{47}$$

It will be convenient to define transformed vibration modes as:

$$\begin{aligned} \tilde{\boldsymbol{\phi}}_1 &= \boldsymbol{\phi}_1 \cos(\varphi) + \boldsymbol{\phi}_2 \sin(\varphi) \\ \tilde{\boldsymbol{\phi}}_2 &= \boldsymbol{\phi}_2 \cos(\varphi) - \boldsymbol{\phi}_1 \sin(\varphi) \end{aligned}, \tag{48}$$

and the frequency responses in the following manner:

$$\begin{aligned} \tilde{H}_1 &= H_1 \cos(\varphi) + H_2 \sin(\varphi) \\ \tilde{H}_2 &= H_2 \cos(\varphi) - H_1 \sin(\varphi) \end{aligned}. \tag{49}$$

The signals s and s' are put through a relay (sign function), and the amplitude control that is presented in Eq. (45). They are then projected on the transformed modes $\tilde{\boldsymbol{\phi}}_1, \tilde{\boldsymbol{\phi}}_2$, resulting in:

$$\begin{aligned} \tilde{\mathbf{s}} &= C_\theta \tilde{\boldsymbol{\phi}}_1 \cos(\omega t) \\ \tilde{\mathbf{s}}' &= -S_\theta \tilde{\boldsymbol{\phi}}_2 \sin(\omega t) \end{aligned}. \tag{50}$$

The projection of the force on the modes of the system, assuming

$$\tilde{H}_1 = \left|\tilde{H}_1\right| e^{i\alpha_1} + cc,\ \tilde{H}_2 = \left|\tilde{H}_2\right| e^{i\alpha_2} + cc, \tag{51}$$

will be:

$$\mathbf{s}_1 = \frac{C_\theta}{2} \tilde{\boldsymbol{\phi}}_1 \left|\tilde{H}_1\right| \left(e^{i(\alpha_1 + \omega t)} + e^{i(\alpha_1 - \omega t)} \right) + cc,\ \mathbf{s}_2 = -\frac{S_\theta}{2i} \tilde{\boldsymbol{\phi}}_2 \left|\tilde{H}_2\right| \left(e^{i(\alpha_2 + \omega t)} - e^{i(\alpha_2 - \omega t)} \right) + cc. \tag{52}$$

Subsequently, modal filtering is applied, resulting in

$$\begin{aligned} s_1 &= C_\theta \tilde{\boldsymbol{H}}_1 \left\| \tilde{\boldsymbol{\phi}}_1 \right\|^2 \cos\left(\omega t + \alpha_1\right) \\ s_2 &= -S_\theta \tilde{\boldsymbol{H}}_2 \left\| \tilde{\boldsymbol{\phi}}_2 \right\|^2 \sin\left(\omega t + \alpha_2\right) \end{aligned} . \tag{53}$$

The functions s_1 and the derivative of s_2 are put through AGC blocks, resulting in uniform amplitude:

$$\begin{aligned} \hat{s}_1 &= \cos\left(\omega t + \alpha_1\right) \\ \hat{s}_2' &= -\cos\left(\omega t + \alpha_2\right) \end{aligned} . \tag{54}$$

The summation of these signals results in:

$$s_{tot} = \hat{s}_1 + \hat{s}_2' = \cos\left(\omega t + \alpha_1\right) - \cos\left(\omega t + \alpha_2\right). \tag{55}$$

For s_{tot} of Eq. (55) to agree with s of Eq. (46), the following relation must hold:

$$\alpha_1 + \alpha_2 = -\pi . \tag{56}$$

Without loss of generality, it is assumed that $\arg(\mathrm{H}_1) < \arg(\mathrm{H}_2)$. Since

$$\alpha_1 = \arg\left(\tilde{H}_1\right) = \arg\left(H_1 \cos(\varphi) + H_2 \sin(\varphi)\right), \tag{57}$$

it can be shown that:

$$\arg\left(H_1\right) \le \arg\left(\tilde{H}_1\right) \le \arg\left(H_2\right). \tag{58}$$

The same can be done for $\arg(\tilde{\mathrm{H}}_2)$. Therefore, for Eq. (56) to hold,

$$\arg\left(H_1\right) > -\pi/2, \arg\left(H_2\right) < -\pi/2, \tag{59}$$

must also be upheld. This implies that the frequency of excitation will be between the two natural frequencies, at a frequency where both modes' amplitudes are high. Therefore, resulting in high amplitudes for the traveling wave, as required. Figure 7 demonstrates the steady-state frequency of excitation for the case graphically when damping is neglected.

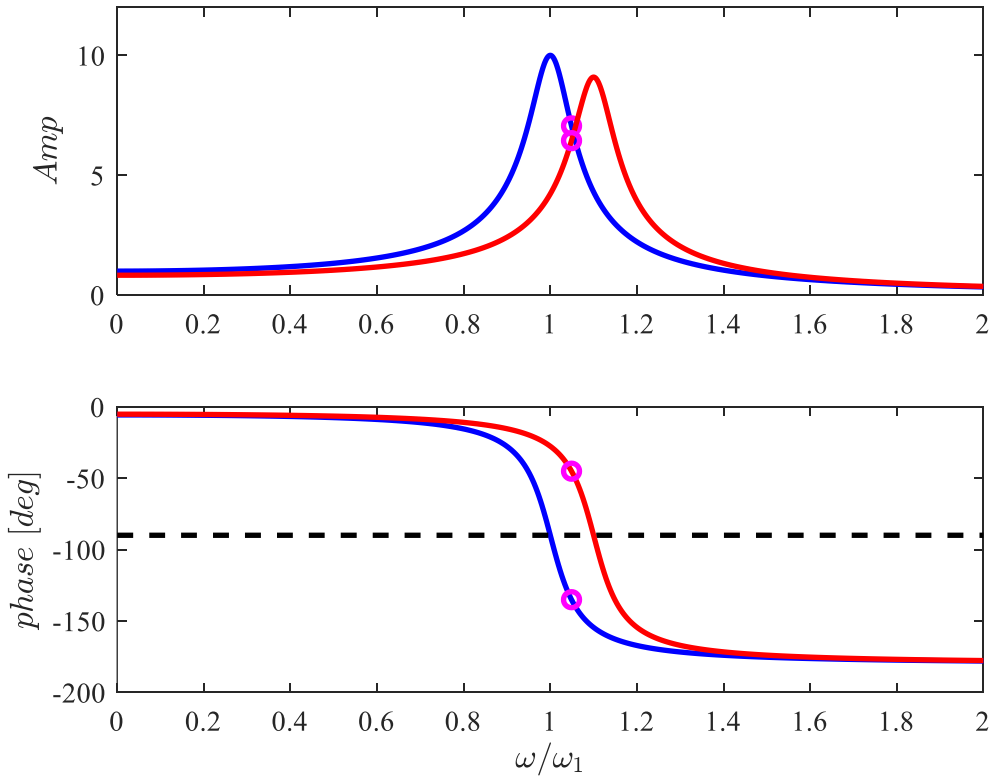

Figure 7 –The frequency response of split doublet modes. In blue – the amplitude and phase of the response of the first mode. In red – the amplitude and phase of the response of the second mode. In black – the phase of -90 degrees, the average phase of both responses must be -90. In magenta – the amplitude and phase of frequency response that has a -90^{o} average phase.

The resulting excitation frequency is close to the average of the two natural frequencies. Therefore, it can be approximated that the frequency of excitation will be

$$\omega \approx \frac{\omega_1 + \omega_2}{2}, \tag{60}$$

where ω_1 and ω_2 are the natural frequencies of the doublet mode. By normalizing the amplitude of excitation by the frequency responses $H_1(\omega)$ and $H_2(\omega)$ using the amplitude control blocks, a pure traveling wave is excited.

4 Optimization of TWA

The described method in section 3 enables propagating pure traveling waves automatically. However, the amplitude of the obtained propagating traveling wave was not discussed. It is of interest to show that the

amplitude of the traveling waves is maximal for the same values of θ and φ. Therefore, ensuring that the presented excitation indeed propagates traveling waves of maximal amplitude. The Traveling Wave Amplitude (TWA) is defined as:

$$\mathrm{TWA} \triangleq \left|U_{+} - U_{-}\right|. \tag{61}$$

Since the TWA is a function of both φ and θ, the maximum will be obtained at:

$$\nabla\left(U_{+} - U_{-}\right) = 0. \tag{62}$$

Taking U_{+}, U_{-} of Eq. (26), (27), and equating $\frac{\partial U_{+}}{\partial \varphi} = \frac{\partial U_{-}}{\partial \varphi}$:

$$\frac{1}{2} S_{2\varphi} \left(\begin{array}{c} \dfrac{C_{2\theta}\Delta_1^2 - 2S_{2\theta}\Delta_1\Delta_2 - C_{2\theta}\Delta_2^2}{\sqrt{\left(\Delta_2 C_\theta C_\varphi + \Delta_1 S_\theta C_\varphi\right)^2 + \left(\Delta_1 C_\theta S_\varphi - \Delta_2 S_\theta S_\varphi\right)^2}} + \\ \dfrac{-C_{2\theta}\Delta_1^2 - 2S_{2\theta}\Delta_1\Delta_2 + C_{2\theta}\Delta_2^2}{\sqrt{\left(\Delta_2 C_\theta C_\varphi - \Delta_1 S_\theta C_\varphi\right)^2 + \left(\Delta_1 C_\theta S_\varphi + \Delta_2 S_\theta S_\varphi\right)^2}} \end{array} \right) = 0. \tag{63}$$

Equation (63) upholds for $\sin(2\varphi) = 0$ which will occur at

$$\varphi = 0, \frac{\pi}{2}, \pi, \tag{64}$$

or for the term in the brackets to be zero. Similarly, equating: $\frac{\partial U_{+}}{\partial \theta} = \frac{\partial U_{-}}{\partial \theta}$:

$$\frac{1}{2} C_{2\varphi} \left(\begin{array}{c} \dfrac{S_{2\theta}\Delta_1^2 - 2C_{2\theta}\Delta_1\Delta_2 - S_{2\theta}\Delta_2^2}{\sqrt{\left(\Delta_2 C_\theta C_\varphi + \Delta_1 S_\theta C_\varphi\right)^2 + \left(\Delta_1 C_\theta S_\varphi - \Delta_2 S_\theta S_\varphi\right)^2}} + \\ \dfrac{-S_{2\theta}\Delta_1^2 + 2C_{2\theta}\Delta_1\Delta_2 + S_{2\theta}\Delta_2^2}{\sqrt{\left(\Delta_2 C_\theta C_\varphi - \Delta_1 S_\theta C_\varphi\right)^2 + \left(\Delta_1 C_\theta S_\varphi + \Delta_2 S_\theta S_\varphi\right)^2}} \end{array} \right) = 0. \tag{65}$$

Equation (65) upholds for $\cos(2\varphi) = 0$, which will occur at $\varphi = \frac{\pi}{4}, \frac{3\pi}{4}$, or for the term in the brackets to be zero. For $\varphi = 0, \frac{\pi}{2}$, the term in the brackets in Eq. (65) must be zero, obtaining:

$$\theta = -\cos^{-1}\left(-\frac{\Delta_1}{\sqrt{\Delta_1^2 + \Delta_2^2}}\right), \cos^{-1}\left(-\frac{\Delta_1}{\sqrt{\Delta_1^2 + \Delta_2^2}}\right), -\cos^{-1}\left(\frac{\Delta_1}{\sqrt{\Delta_1^2 + \Delta_2^2}}\right), \cos^{-1}\left(\frac{\Delta_1}{\sqrt{\Delta_1^2 + \Delta_2^2}}\right). \tag{66}$$

These sets of parameters are identical to the ones for which TWR=0 is obtained. For $\varphi = \frac{\pi}{4}, \frac{3\pi}{4}$, the following solutions are obtained:

$$\theta = -\frac{\pi}{2}, 0, \frac{\pi}{2}. \tag{67}$$

These values will result in the excitation of a pure standing wave, which will obtain minimum TWA. Therefore, for the chosen excitation, the maximal amplitude of a traveling wave is obtained for the set of parameters found in Eq. (64) and Eq. (66). As seen in Eq. (28), the same parameters result in a TWR=0. These findings show that whether the goal is to create maximal amplitude of the traveling wave, or to propagate a pure traveling wave, the optimization procedure of the parameters φ, θ is identical.

5 Ultrasonic actuator simulation

The proposed method was numerically simulated on an ultrasonic actuator designed to utilize traveling waves to control the rotation of acoustically levitated objects. An ANSYS FE software model of the actuator is presented in Figure 8. The annulus was modeled as an aluminum ring with an inner diameter of 100 mm, outer diameter of 150 mm, and 5 mm thickness. Reference [2] suggested an open-loop form of actuation, controlling the phases to produce the desired TWR. While Ref. [33] introduced a Modal Filtering autoresonance (MFAR) to track the system's natural frequency. In both papers, the system model assumed cyclic symmetry, and the actuator was designed, manufactured, and assembled under high tolerances to ensure that the system maintains cyclic symmetry. The method presented in this paper is designed to overcome imperfections in the system, a situation that was not addressed in the previous papers. A significant defect in the actuator is desirable to examine the proposed method's success. Therefore, a simulation was performed in which a defect could be introduced easily without harming the physical actuator. In addition, a simulation allows measuring the system's full response and consequently obtaining the actual TWR. Hence, based on the numerical simulation results, a comparison with the real-time approximation of the TWR using the proposed filter is carried.

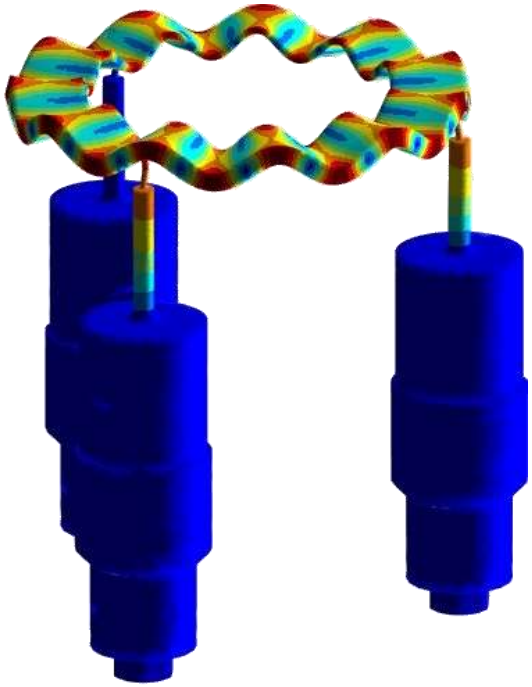

Figure 8 - A finite element simulation of a mode shape of the acoustic levitation ring. The ring is actuated and measured at 3 points located 120 degrees from each other.

The mass and stiffness matrix of the ring were exported to MATLAB. Then, the stiffness matrix corresponding to the nodes in the area shown in Figure 9 was altered to be 90% of the original one. This type of perturbation causes a shift in the natural frequency, while the spatial distribution of the mode shapes is not altered significantly and can be still approximated as sine and cosine functions.

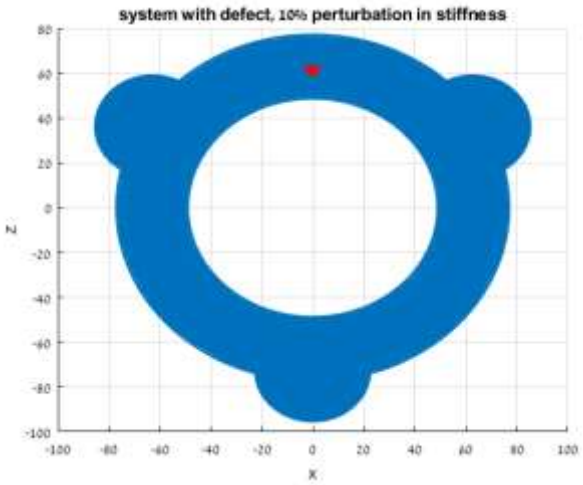

Figure 9 – Top view of the ring. The red area represents a change in nominal stiffness of 10 percent.

The excitation force of the system is in the form presented in Eq. (12), at the 3 actuation locations. The values of φ and θ, are varied, and a frequency of excitation between the doublet modes (split) natural frequencies is used. The TWR and TWA were approximated using Eq. (2) and (61). Magnitude maps of the TWR and TWA of the system for different excitations were constructed. The maps are presented in Figure 10

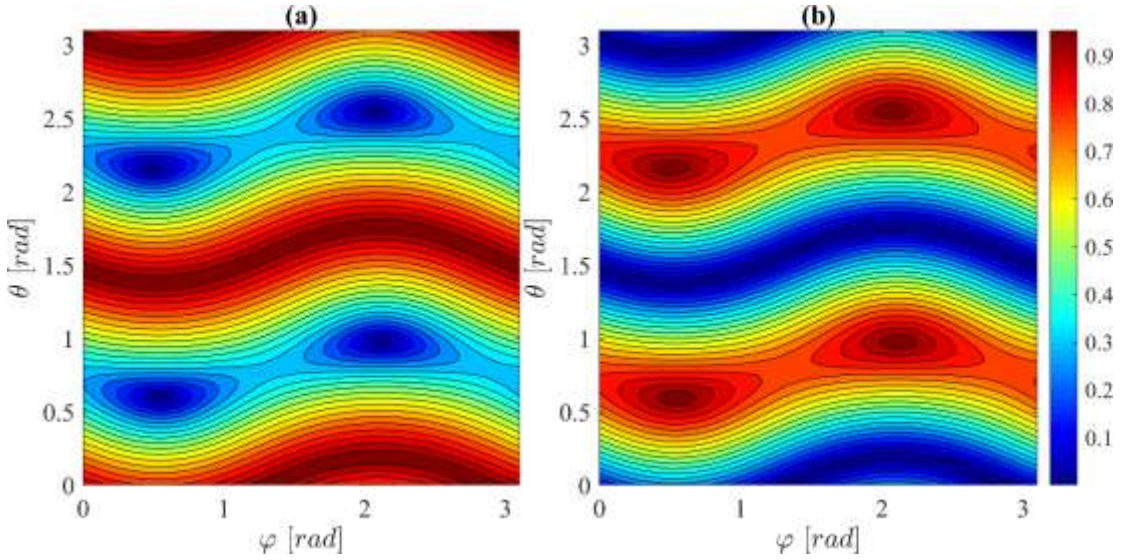

Figure 10 – The simulated maps for the excitation of the ultrasonic levitation actuator. 4 identical extremum points can be identified on each map. (a) The simulated TWR map. Dark blue represents TWR=0 (traveling wave), while red represents TWR=1 (standing wave). (b) The simulated normalized TWA map. Red represents maximal TWA, while blue represents minimal TWA.

From Figure 10, it can be deduced that the TWR and TWA are at extremum for the same values of φ and θ as expected. In addition, the differences between the amplitudes of the traveling wave for the different extremum points are under 4%, showing that the damping did not drastically change the analysis of section 3.

The system was excited via a Simulink™ simulation of the proposed TWAR method, assuming sensing is possible at the 3 actuation points. The TWR is approximated using the filtering proposed in section 3.1. The time history of the estimated TWR is shown in Figure 11.

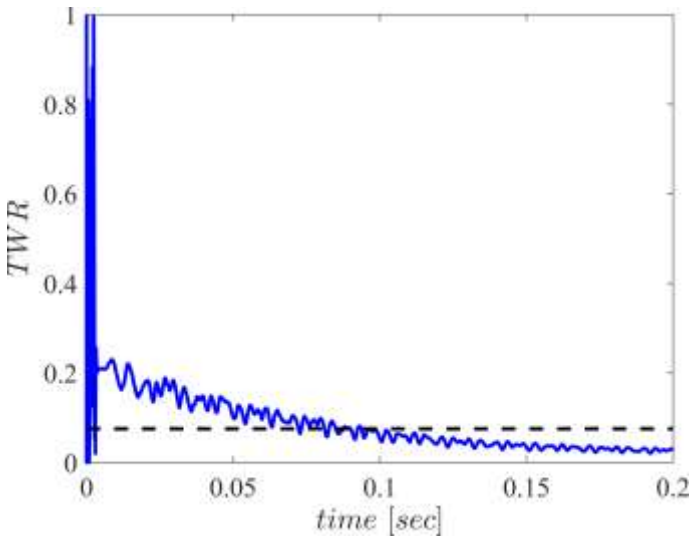

Figure 11 – In blue, the evaluated TWR, used as a cost function for the extremum seeking control loop. In black, the approximated TWR using the full response of the simulated system.

The steady-state response of the system was extracted, and the TWR of the entire system was calculated, resulting in TWR=0.0816, while the TWR evaluated using the filter is 0.0278. These results validate the ability to use the TWAR method on continuous systems with multiple modes, using limited means of excitation and sensing. It is evident that the form of excitation suggested for the nominal system ($\theta = 45, \varphi = 120$ degrees [34]) without the defect results in a sub-optimal result of TWR=0.2. The use of TWAR-control results in an 8dB attenuation of the TWR. These results validate the effectiveness of the proposed method.

6 Experimental results

6.1 Experimental system

The experimental system of an acoustic ring of 12 HRs (Helmholtz resonators) used to verify the developed method is presented in Figure 12. Each HR consists of a cavity and two necks, as presented in Figure 12(a). An actuator (loudspeaker) and a sensor (microphone) are connected to each cavity. The entire experimental system is presented in Figure 12 (b).

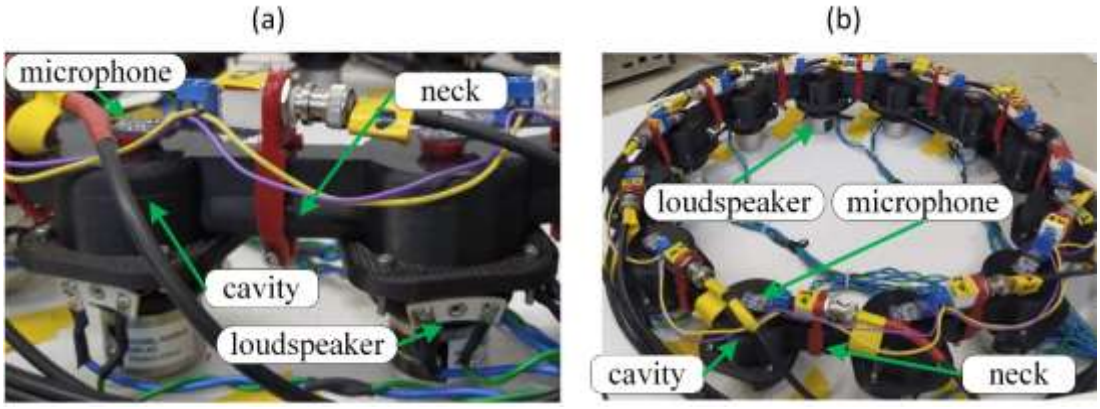

Figure 12- The experimental system. (a) – Two HR cells, connected by their necks. The neck is modeled as a lumped mass. The cavities are modeled as linear springs. (b) – A photograph of the experimental system, which consists of 12 HR cells connected by their necks, actuated by 12 loudspeakers, and measured using 12 microphones.

As shown in [41], considering a ring of N HRs with uniform necks and cavities, the n^{th} equation will take the form of:

$$\ddot{x}_n + \frac{c^2 A}{v_0 l}\left(2x_n - x_{n-1} - x_{n+1}\right) = Q_n - Q_{n-1},\ n = 1,\cdots,N, \tag{68}$$

where due to the cyclic nature $n = 0 \to n = N$, and $n = N + 1 \to n = 1$. Actuation and control of the system were implemented on the odd-numbered HRs (x_{2n-1}). Due to the difference in the impedance of the actuated and un-actuated cells, a skyhook is added to each even cell, modifying the unit cell to be of the form presented in Figure 13.

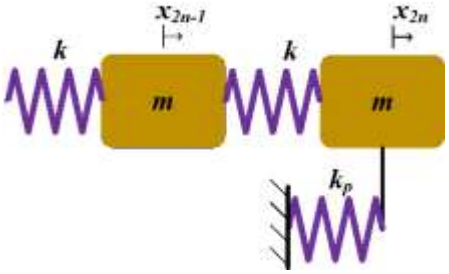

Figure 13 – The model of the modified unit cell due to partial actuation of the system.

The modified 2n$^{\text{th}}$ EOM becomes:

$$\ddot{x}_n + \frac{c^2 A}{v_0 l}\left(\left(2 + k_p\right)x_{2n} - x_{2n-1} - x_{2n+1}\right) = Q_n - Q_{n-1},\ n = 1,\cdots,N, \tag{69}$$

where k_p represents the added stiffness. Since the system maintains cyclic symmetry, the first mode shape at a periodic point in the unit cell still upholds [39]:

$$\phi_{n,r} = \mathrm{Re}\left(A_r e^{i\frac{2\pi n}{N}} \right), r = 1,2\,. \tag{70}$$

Therefore, Eq. (1) is updated to be:

$$\begin{bmatrix} u(q_{2n-1},t) \\ u(q_{2n},t) \end{bmatrix} = \Re\left(\begin{bmatrix} 1 \\ A \end{bmatrix} U_+ e^{i(\omega t - \kappa q_n)} + \begin{bmatrix} 1 \\ \bar{A} \end{bmatrix} U_- e^{i(\omega t + \kappa q_n)} \right), n = 1 \ldots N\,, \tag{71}$$

where A is the complex amplitude of the un-actuated cavities in the unit cell and $\bar{A}$ is its complex conjugate. Although the model of Eq. (69) assumes that the system is cyclically symmetric, this is not true for the experimental system, as will be shown and discussed in section 6.2.

6.2 Open-loop map

It is of interest to validate the findings of section 3 and ensure that there are four combinations of φ and θ for pure traveling wave propagation. Thus, an open-loop map of the TWR was constructed based on data obtained from the HR experiment actuated with different sets of θ and φ. The TWR map is shown in Figure 14(a). In addition, a detuned simulation based on Eq. (68) with the edition of a 10% change in one of the spring's stiffnesses was used to obtain a similar TWR map shown in Figure 14(b).

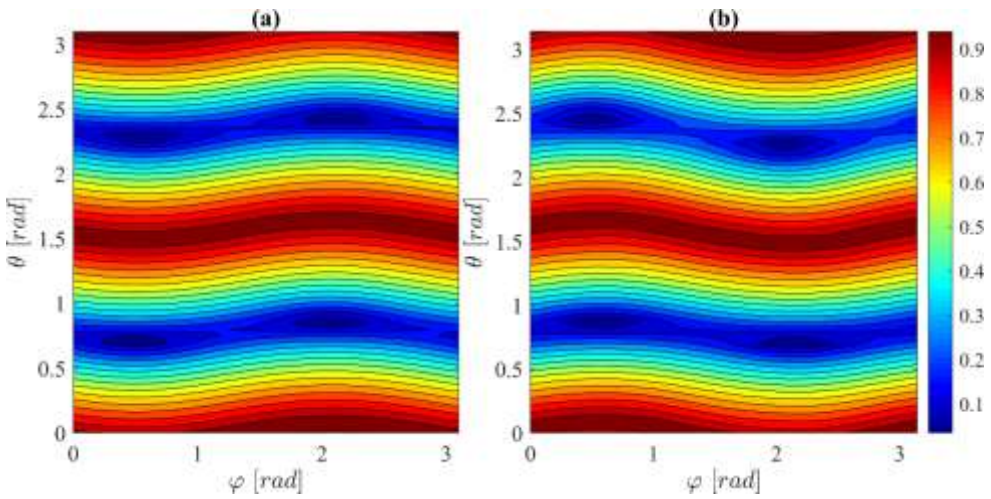

Figure 14 – Maps of TWR for different combinations of φ and θ. Dark blue represents TWR=0. Red represents TWR=1. There are 4 points of TWR=0, as found analytically. (a) Measured response. (b) Simulated response.

Figure 14(a) shows the experimentally obtained TWR map. Note that the experimental system TWR is at minimum for exactly 4 different combinations of θ and φ as predicted in Section 3. Also, the detuned model simulation TWR (Figure 14(b)) is in good agreement with the experimentally obtained one, indicating that the experimental system is indeed not cyclic symmetric. In addition, there is a phase difference between the values of φ, due to different points of perturbation. This results in a different initial phase φ_0 from Eq. (8), of the perturbed mode shapes. Therefore, classical approaches to control and propagate pure traveling waves that assume uniform amplitude and phase of the doublet modes will yield suboptimal results.

6.3 Simulated and Experimental results of TWR optimization

The following subsection presents the results of optimization of propagation of traveling waves using the AR excitation as described in Figure 2. The control method presented in section 3 was constructed using Simulink and implemented on a dSPACE™ processor, which controlled the actuation of the system using the sensors as inputs. The TWAR, which was introduced in subsection 3.3, was used to excite the system, and the filter presented in subsection 3.1 was used to approximate the TWR of the system. Extremum seeking, as presented in subsection 3.2, was used to control the amplitude control and modal filter blocks of the TWAR, to obtain TWR=0. The frequencies of perturbation for extremum seeking were set to $\frac{1}{5}$ Hz

for the amplitude control (θ) and $\frac{1}{3}$ Hz for the modal filtering control (φ). The LPF for the approximation of the TWR is a second-order IIR with a cutoff frequency of 16 Hz. These values were chosen to ensure that the system and the TWR approximation filter reached steady-state and were chosen based on the calibrated simulation. The simulation was performed on an imperfect system similar to the one presented in Figure 1, and the experiments were executed on the imperfect experimental system presented in Figure 12.

The results for the simulation of TWR optimization with AR excitation using the parameters θ and φ are presented in Figure 15.

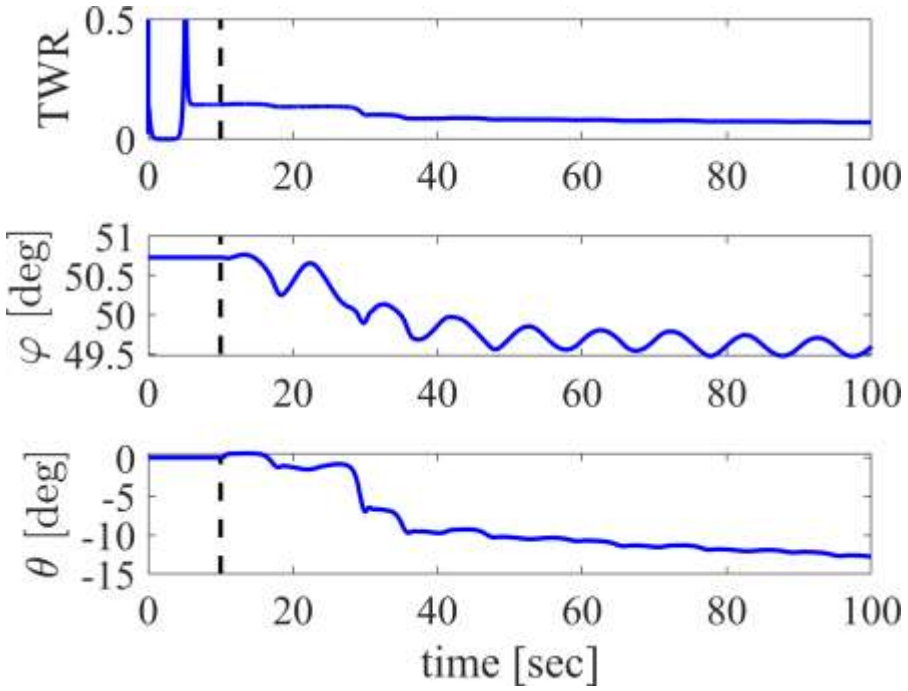

Figure 15 –The simulated response of extremum seeking for two parameters. The control loop initiated at t=10 (in black). The cost function of the TWR arrives at 0, and the optimized parameters φ and θ reach steady state with small oscillations. The simulation verifies the ability to optimize both parameters simultaneously and achieve low values of TWR.

The optimization begins after 10 seconds when the TWR filter reaches its steady state. Oscillations of the optimized parameters due to the extremum seeking method are observed, though their amplitude is proportional to the TWR magnitude. The TWR decreased from a value of 0.15 to approximately 0.07. The TWR is not 0 because θ is not yet at steady state, and since at steady state there still are small oscillations, the TWR is not optimal.

The method of extremum seeking was used on the experimental system, yielding the results presented in Figure 16:

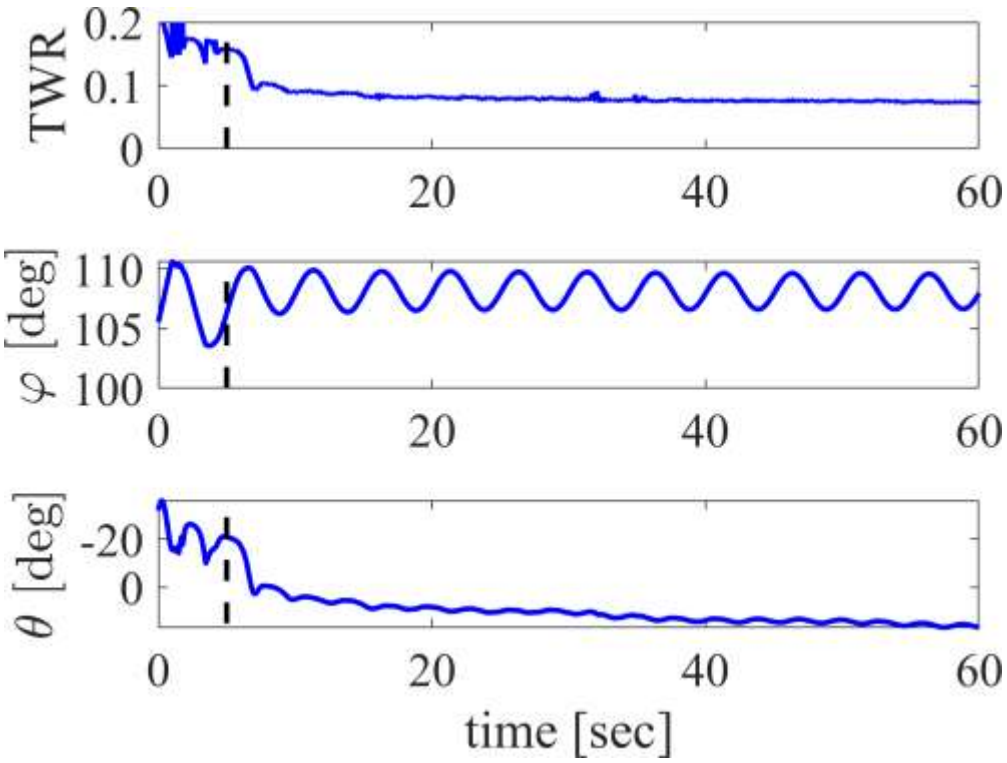

Figure 16 – Experimental results. The control loop initiated at t=4 (in black). The cost function of the TWR arrives at 0, and the optimized parameters φ and θ reach steady state with small oscillations, due to the extremum seeking method's induced perturbations.

It can be observed that the parameters oscillate and are gradually optimized to values that result in a low TWR. Here too, the improvement is approximately 50% in the TWR. The signal in time of the 12 microphones at steady state is presented in Figure 17:

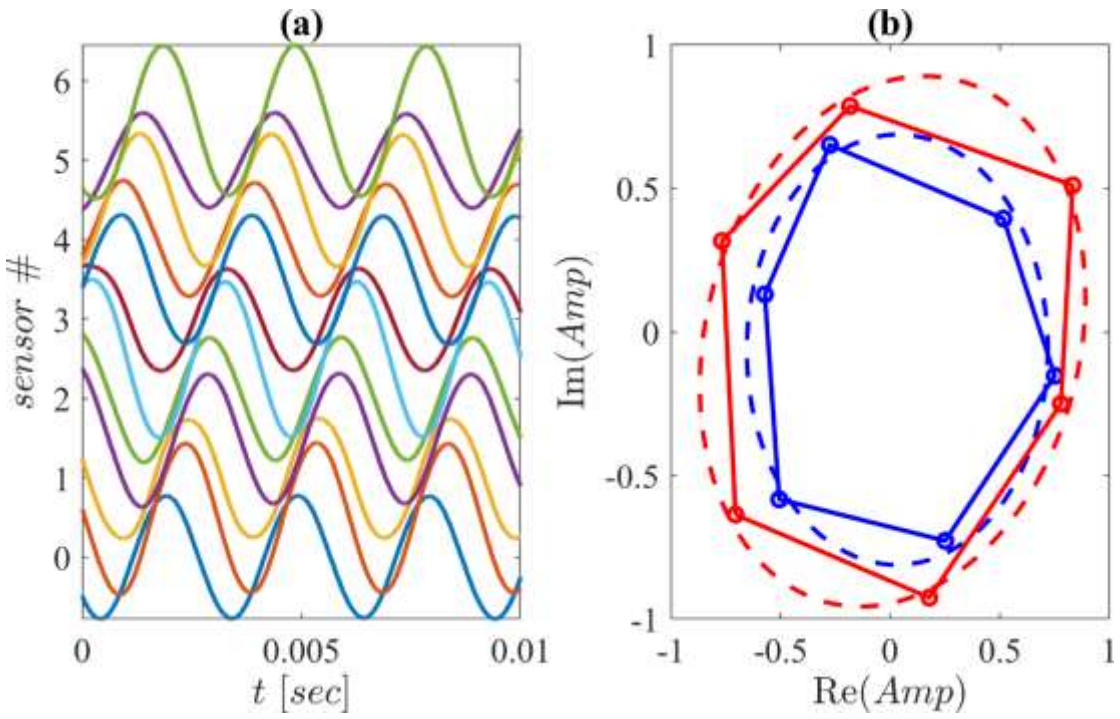

Figure 17 – (a) The signals in time. The traveling wave propagates through the DOF. Higher frequencies can be observed due to small nonlinearities in the system and the nonlinearity of the AR loop. (b) Real vs Imaginary part of complex amplitudes. 2 ellipses are fitted, one for each sub-unit in the cyclic symmetric unit cell.

As proposed in Eq. (71), the system's response consists of two components, forming two ellipses. It has been shown that propagating waves with traveling and standing components form an ellipse when their amplitude is plotted on the complex plane [45]. A pure standing wave will result in a straight line (constant phase), while a pure traveling wave results in a perfect circle (constant amplitude). Since the response presented in Figure 17 (b) is close to 2 circles, it is evident that a traveling wave propagates in the system. Therefore, validating the assumption that a partial excitation will be sufficient to excite traveling waves in the system.

It is worth noting that the simulation and experiment convergence times are relatively long. This is due to some factors: firstly, the dynamics of the system are slow relative to ultrasonic systems. This can be seen in Figure 11, where for the acoustic levitation ring, which has higher natural frequencies, convergence is at 0.2 seconds. Secondly, the method overcomes a large defect, in comparison with the variations of the dynamics of systems over time, which are typically slow. In addition, since the TWR improves almost immediately, the results validate the efficiency of this method.

6.4 Optimization of TWA

To validate the findings of section 4, that the TWR and TWA obtain extremum for the same combinations of φ and θ, TWR and TWA maps were experimentally constructed at each frequency of excitation. An example of a map of the TWR and TWA is presented in Figure 18:

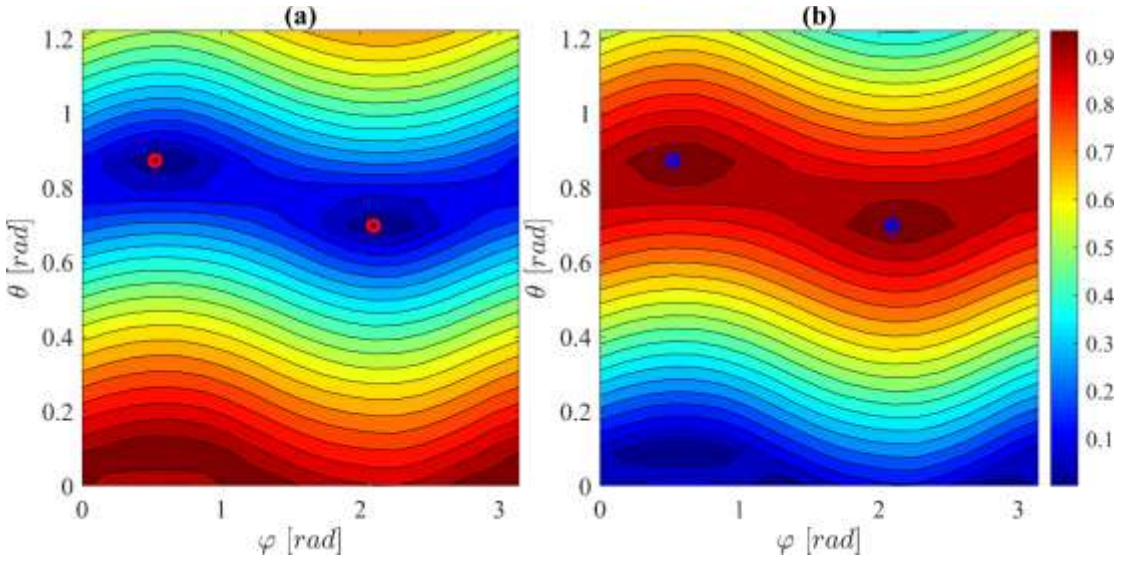

Figure 18 –The TWR(a) and TWA(b) maps in the vicinity of 2 extremum points. The red points represent the extremum of the TWR, and the blue points represent the extremum of the TWA.

The TWR and TWA obtain extremum at each frequency for the same combinations of φ and θ, as presented in Figure 19:

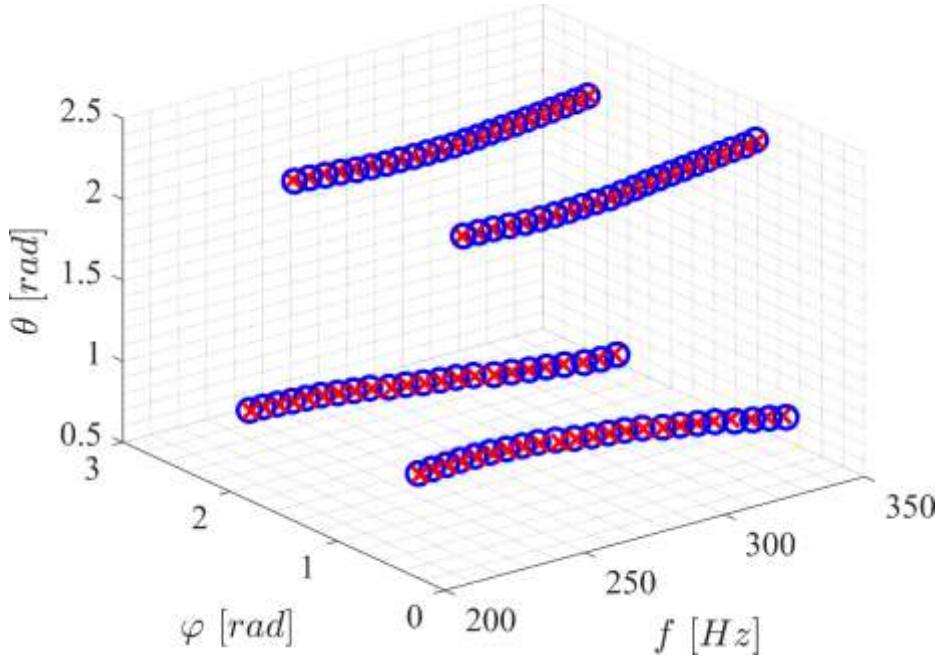

Figure 19- The optimal values of φ and θ for each frequency of excitation, for optimal TWR in red crosses and TWA in blue circles.

From these results, it is evident that the parameters φ and θ achieve maximal amplitudes and TWR=0 at the same points, as predicted. This validates the analysis presented in section 4, which concluded that the maximal amplitude of the traveling wave for a given amplitude of excitation is achieved with the same parameters resulting in TWR=0. Therefore, when maximal TWA is desired, it is sufficient to achieve TWR=0.

7 conclusions

This paper outlines an adaptive tuning method of excitation to produce a pure traveling wave in imperfect cyclic symmetric systems. The method uses adaptive control to optimize the two phases of excitation θ and φ that, when tuned to the appropriate values, were proved to result in a pure traveling wave. The frequency of excitation was obtained using the traveling wave autoresonance, which locks on to a frequency between the natural frequencies of the excited doublet modes. This method was verified using simulations, and experimentally on an acoustic cyclic symmetric system. The results show low TWR, which indicates that the method succeeds in exciting traveling waves. The adaptive form of excitation enables the system to automatically lock on to optimal excitation variables and a frequency between the split doublet modes' resonance frequencies. In addition, it was shown analytically and verified numerically that the control parameters achieve maximal amplitude and pure traveling waves together.

Appendix A – Time phase excitation

When it is impossible to control the distribution of the actuation (e.g. in USM using to 2 actuation inputs), a time-induced phase between the cosine and sine components of the excitation can be introduced in the form of:

$$\mathbf{F}=\cos(\theta)\cos(\kappa\mathbf{s})\left(e^{i(\omega t-\varphi)}+e^{-i(\omega t-\varphi)}\right)-i\sin(\theta)\sin(\kappa\mathbf{s})\sin\left(e^{i(\omega t+\varphi)}+e^{-i(\omega t+\varphi)}\right). \tag{72}$$

The modes are assumed to be sinusoidal with some initial phase γ :

$$\boldsymbol{\phi}_1=\cos(\kappa\mathbf{s}+\gamma),\ \boldsymbol{\phi}_2=\sin(\kappa\mathbf{s}+\gamma). \tag{73}$$

The response of the system will be of the form:

$$\mathbf{q}(\omega)=\begin{pmatrix}\boldsymbol{\phi}_1\begin{pmatrix}\left(|H_1|C_{\alpha_1}\left(C_\gamma C_\theta C_\varphi-S_\gamma S_\theta S_\varphi\right)+|H_1|S_{\alpha_1}\left(C_\gamma C_\theta S_\varphi-S_\gamma S_\theta C_\varphi\right)\right)\cos(\omega t)\\+\left(|H_1|C_{\alpha_1}\left(C_\gamma C_\theta S_\varphi-S_\gamma S_\theta C_\varphi\right)+|H_1|S_{\alpha_1}\left(C_\gamma C_\theta C_\varphi-S_\gamma S_\theta S_\varphi\right)\right)\sin(\omega t)\end{pmatrix}+\\ \boldsymbol{\phi}_2\begin{pmatrix}\left(-|H_2|C_{\alpha_2}\left(S_\gamma C_\theta C_\varphi+C_\gamma S_\theta S_\varphi\right)+|H_2|S_{\alpha_2}\left(S_\gamma C_\theta S_\varphi+C_\gamma S_\theta C_\varphi\right)\right)\cos(\omega t)\\+\left(|H_2|C_{\alpha_2}\left(S_\gamma C_\theta S_\varphi+C_\gamma S_\theta C_\varphi\right)+|H_2|S_{\alpha_2}\left(S_\gamma C_\theta C_\varphi+C_\gamma S_\theta S_\varphi\right)\right)\sin(\omega t)\end{pmatrix}\end{pmatrix}. \tag{74}$$

By nullifying the forward-going component of the response, the following set of equations is obtained:

$$\begin{pmatrix}\left(|H_1|C_{\alpha_1}\left(C_\gamma C_\theta C_\varphi-S_\gamma S_\theta S_\varphi\right)+|H_1|S_{\alpha_1}\left(C_\gamma C_\theta S_\varphi-S_\gamma S_\theta C_\varphi\right)+\right.\\ \left.\left(|H_2|C_{\alpha_2}\left(S_\gamma C_\theta S_\varphi+C_\gamma S_\theta C_\varphi\right)+|H_2|S_{\alpha_2}\left(S_\gamma C_\theta C_\varphi+C_\gamma S_\theta S_\varphi\right)\right)\right)=0\\ \left(\left(|H_2|C_{\alpha_2}\left(S_\gamma C_\theta C_\varphi+C_\gamma S_\theta S_\varphi\right)+|H_2|S_{\alpha_2}\left(S_\gamma C_\theta S_\varphi+C_\gamma S_\theta C_\varphi\right)\right)-\right.\\ \left.\left(|H_1|C_{\alpha_1}\left(C_\gamma C_\theta S_\varphi-S_\gamma S_\theta C_\varphi\right)+|H_1|S_{\alpha_1}\left(C_\gamma C_\theta C_\varphi-S_\gamma S_\theta S_\varphi\right)\right)\right)=0\end{pmatrix}. \tag{75}$$

Similar to the derivation shown in section 2, it is possible to extract from this set of equations combinations of θ and φ that produce a pure traveling wave. These values can be obtained using extremum seeking control, as done in section 3.

TWR maps were constructed for different values of γ to show the ability to propagate traveling waves (Figure 20):

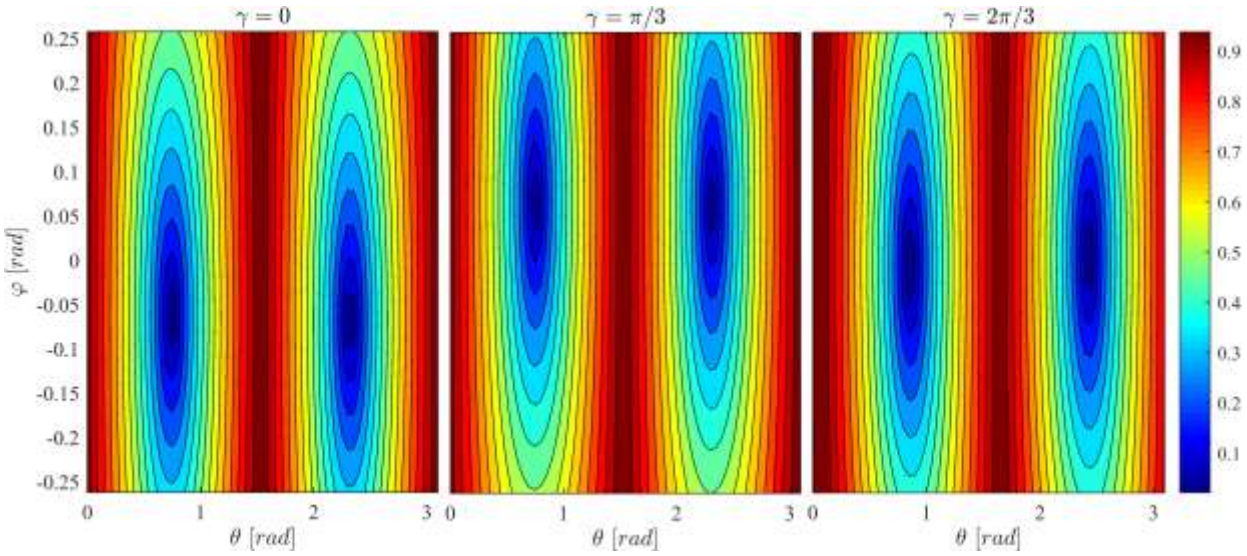

Figure 20 – The TWR maps using time phase excitation for $\gamma = 0, \gamma = \pi/3$, and $\gamma = 2\pi/3$

For each value of γ that was used, two combinations of φ and θ resulting in TWR=0 were found.

Appendix B – The response of a single degree of freedom system to autoresonance excitation

Following [28], a block diagram of the AR loop is presented in Figure 21.

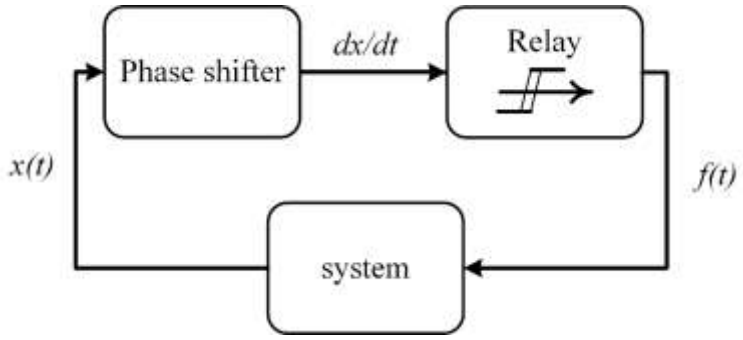

Figure 21 – AR feedback for a single degree of freedom.

The system for which the AR is being applied is a single degree of freedom (SDOF) system,

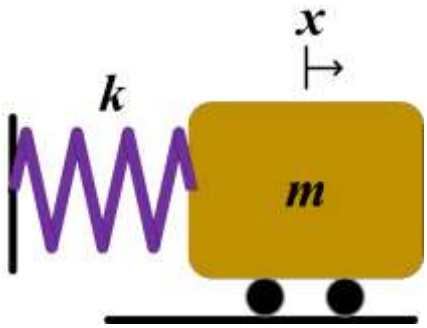

Figure 22- A diagram of a SDOF system. The coordinate x represents the displacement of the mass m.

with the equation of motion:

$$\ddot{x} + 2\zeta\omega_n + \omega_n^2 x = 0, \tag{76}$$

where x is the coordinate describing the displacement of the system, and ω_n is the natural frequency of the system, $\omega_n = \sqrt{k/m}$. The relay acts as a step response with the amplitude of 1, exciting the system in oscillations of

$$\tilde{x}(t) = 1 - e^{-\zeta\omega_n t}\cos\left(\omega_d \tilde{t} + \phi_0\right). \tag{77}$$

By shifting the time variable to be $t = \tilde{t} - \frac{\phi_0}{\omega_d}$, the response becomes:

$$x = 1 - \cos\left(\omega_d t\right). \tag{78}$$

After putting the system through -1 gain and a phase shifter, the signal becomes:

$$s \approx e^{-\zeta\omega_n t}\sin\left(\omega_d t\right). \tag{79}$$

The signal coming out of the relay will be:

$$f(t) = sign\left(\sin\left(\omega_d t\right)\right). \tag{80}$$

This signal will change sign when $t = \frac{\pi}{\omega_d}$, resulting in

$$x = 1 + e^{-\zeta\pi} \triangleq A_0, \dot{x} = 0. \tag{81}$$

These are the initial conditions for the step response coming from the sign function. The response of a SDOF system to a step function with the amplitude of -1 with the initial conditions shown in Eq. (81) will be:

$$-1 + A_0 e^{-\zeta\omega_n t}\cos\left(\omega_d t\right). \tag{82}$$

The signal coming out of the relay will now be:

$$\tilde{s} = -sign\left(\sin\left(\omega_d t\right)\right), \tag{83}$$

which will switch from -1 to 1 for $t = \frac{\pi}{\omega_d}$, for which the state of the system will be:

$$x = -\left(1 + e^{-\zeta\pi} + e^{-\zeta 2\pi}\right), \dot{x} = 0. \tag{84}$$

The system has arrived at the same initial conditions as in the beginning, indicating a limit cycle with the frequency of oscillations ω_d. The maximal amplitude will be of the series $1 + e^{-\zeta\pi} + e^{-2\zeta\pi} + \cdots$, and the amplitude at steady state will be:

$$A_{ss} = \frac{1}{1 - e^{-\zeta\pi}}. \tag{85}$$

Acknowledgments

The second author, Y. Vered, is supported by the UK Engineering and Physical Sciences Research Council (EPSRC) through the DigiTwin project (grant EP/R006768/1).

References

[1] X. Lu, J. Hu, L. Yang, C. Zhao, A novel dual stator-ring rotary ultrasonic motor, Sensors Actuators, A Phys. (2013). https://doi.org/10.1016/j.sna.2012.11.009.

[2] R. Gabai, D. Ilssar, R. Shaham, N. Cohen, I. Bucher, A rotational traveling wave based levitation device – Modelling, design, and control, Sensors Actuators, A Phys. (2017). https://doi.org/10.1016/j.sna.2016.12.016.

[3] Y. Vered, I. Bucher, Nonlinear control of boundary impedance in an acoustic waveguide, J. Acoust. Soc. Am. 150 (2021) 3889–3903. https://doi.org/10.1121/10.0007228.

[4] S. Backhaus, E. Tward, M. Petach, Traveling-wave thermoacoustic electric generator, Appl. Phys. Lett. (2004). https://doi.org/10.1063/1.1781739.

[5] Z. Zhang, S. Zheng, X. Jin, H. Chi, X. Zhang, Generation of Plane Spiral OAM Waves Using Traveling-Wave Circular Slot Antenna, IEEE Antennas Wirel. Propag. Lett. (2017). https://doi.org/10.1109/LAWP.2016.2552227.

[6] Jones, Keith W., and Charles J. Cross. "Traveling wave excitation system for bladed disks." *Journal of propulsion and power* 19.1 (2003): 135-141. https://doi.org/10.2514/2.6089.

[7] Zhuo, C., Zhang, H., Samanta, R., Hu, J., & Chen, K. (2007, November). Modeling, optimization and control of rotary traveling-wave oscillator. In *2007 IEEE/ACM International Conference on Computer-Aided Design* (pp. 476-480). IEEE. https://doi.org/10.1109/ICCAD.2007.4397310

[8] S.N. Chow, J. Mallet-Paret, W. Shen, Traveling Waves in Lattice Dynamical Systems, J. Differ. Equ. (1998). https://doi.org/10.1006/jdeq.1998.3478.

[9] M. Endo, K. Hatamura, M. Sakata, O. Taniguchi, Flexural vibration of a thin rotating ring, J. Sound Vib. (1984). https://doi.org/10.1016/0022-460X(84)90560-1.

[10] C.C. Glynn, On the resonant nonlinear traveling waves in a thin rotating ring, Int. J. Non. Linear. Mech. (1982). https://doi.org/10.1016/0020-7462(82)90003-8.

[11] H. Plat, I. Bucher, Parametric excitation of traveling waves in a circular non-dispersive medium, J. Sound Vib. (2014). https://doi.org/10.1016/j.jsv.2013.11.005.

[12] J.Y. Chang, J.A. Wickert, Response of modulated doublet modes to travelling wave excitation, J. Sound Vib. 242 (2001) 69–83. https://doi.org/10.1006/jsvi.2000.3363.

[13] S. Jingzhuo, L. Yu, H. Jingtao, X. Meiyu, Z. Juwei, Z. Lei, Novel intelligent PID control of traveling wave ultrasonic motor, ISA Trans. 53 (2014) 1670–1679. https://doi.org/10.1016/J.ISATRA.2014.05.022.

[14] M. Kuhne, R.G. Rochin, R.S. Cos, G.J.R. Astorga, A. Peer, Modeling and Two-Input Sliding Mode Control of Rotary Traveling Wave Ultrasonic Motors, IEEE Trans. Ind. Electron. 65 (2018) 7149–7159. https://doi.org/10.1109/TIE.2018.2798570.

[15] L. Song, S. Jingzhuo, Novel Generalized Predictive Iterative Learning Speed Controller for Ultrasonic Motors, IEEE Access. 8 (2020) 29344–29353. https://doi.org/10.1109/ACCESS.2020.2972940.

[16] A. Ferreira, P. Minotti, High-performance load-adaptive speed control for ultrasonic motors,

Control Eng. Pract. 6 (1998) 1–13. https://doi.org/10.1016/S0967-0661(97)10057-0.

[17] F.R. Mohd Romlay, W.A. Wan Yusoff, K.A. Mat Piah, Increasing the efficiency of traveling wave ultrasonic motor by modifying the stator geometry, Ultrasonics. 64 (2016) 177–185. https://doi.org/10.1016/J.ULTRAS.2015.09.002.

[18] W. Shi, H. Zhao, J. Ma, Y. Yao, Optimal working frequency of ultrasonic motors, Ultrasonics. 70 (2016) 38–44. https://doi.org/10.1016/J.ULTRAS.2016.04.015.

[19] Senjyu, Tomonobu, Satoru Yokoda, and Katsumi Uezato. "A study on high-efficiency drive of ultrasonic motors." *Electric Power Components and Systems* 29.3 (2001): 179-189. https://doi.org/10.1080/153250001300006617.

[20] W. Shi, H. Zhao, J. Ma, Y. Yao, An Optimum-Frequency Tracking Scheme for Ultrasonic Motor, IEEE Trans. Ind. Electron. 64 (2017) 4413. https://doi.org/10.1109/TIE.2017.2674612.

[21] J. Judge, C. Pierre, O. Mehmed, Experimental investigation of mode localization and forced response amplitude magnification for a mistuned bladed disk, J. Eng. Gas Turbines Power. (2001). https://doi.org/10.1115/1.1377872.

[22] Wei, S-T., and C. Pierre. "Localization phenomena in mistuned assemblies with cyclic symmetry part ii: Forced vibrations." (1988): 439-449. https://doi.org/10.1115/1.3269548

[23] D. Zhang, S. Wang, J. Xiu, Distorted wave response of ultrasonic annular stator incorporating non-uniform geometry, Wave Motion. 68 (2017) 43–55. https://doi.org/10.1016/J.WAVEMOTI.2016.08.008.

[24] Y. Vered, I. Bucher, Experimental multimode traveling waves identification in an acoustic waveguide, Mech. Syst. Signal Process. 153 (2021) 107515. https://doi.org/10.1016/j.ymssp.2020.107515.

[25] K.B. Ariyur, M. Krstic, Real-time optimization by extremum-seeking control, John Wiley & Sons, 2003.

[26] R. Leyva, C. Alonso, I. Queinnec, A. Cid-Pastor, D. Lagrange, L. Martínez-Salamero, MPPT of

photovoltaic systems using extremum - Seeking control, IEEE Trans. Aerosp. Electron. Syst. (2006). https://doi.org/10.1109/TAES.2006.1603420.

[27] Killingsworth, N., and M. Krstic. *PID tuning using extremum seeking*. No. UCRL-JRNL-217161. Lawrence Livermore National Lab.(LLNL), Livermore, CA (United States), 2005. https://doi.org/10.1109/MCS.2006.1580155.

[28] Aström, Karl Johan, Graham Clifford Goodwin, and Panqanamala Ramana Kumar, eds. *Adaptive control, filtering, and signal processing*. Vol. 74. Springer Science & Business Media, 2012.

[29] V.I. Babitsky, Autoresonant mechatronic systems, Mechatronics. (1995). https://doi.org/10.1016/0957-4158(95)00026-2.

[30] E. Rubin, S. Davis, I. Bucher, Multidimensional topography sensing simulating an AFM, Sensors Actuators, A Phys. 303 (2020). https://doi.org/10.1016/j.sna.2019.111690.

[31] V.I. Babitsky, V.K. Astashev, A.N. Kalashnikov, Autoresonant control of nonlinear mode in ultrasonic transducer for machining applications, Ultrasonics. 42 (2004) 29–35.

[32] I.J. SOKOLOV, V.I. BABITSKY, PHASE CONTROL OF SELF-SUSTAINED VIBRATION, J. Sound Vib. 248 (2001) 725–744. https://doi.org/10.1006/jsvi.2001.3810.

[33] S. Davis, I. Bucher, Automatic vibration mode selection and excitation; combining modal filtering with autoresonance, Mech. Syst. Signal Process. 101 (2018) 140–155. https://doi.org/10.1016/j.ymssp.2017.08.009.

[34] S. Davis, R. Gabai, I. Bucher, Realization of an automatic, contactless, acoustic levitation motor via degenerate mode excitation and autoresonance, Sensors Actuators, A Phys. 276 (2018) 34–42. https://doi.org/10.1016/j.sna.2018.03.021.

[35] R.L. Panton, J.M. Miller, Resonant frequencies of cylindrical Helmholtz resonators, J. Acoust. Soc. Am. 57 (1975) 1533–1535. https://doi.org/10.1121/1.380596.

[36] M.B. Xu, A. Selamet, H. Kim, Dual Helmholtz resonator, Appl. Acoust. 71 (2010) 822–829. https://doi.org/10.1016/J.APACOUST.2010.04.007.

[37] Géradin, Michel, and Daniel J. Rixen. *Mechanical vibrations: theory and application to structural dynamics*. John Wiley & Sons, 2014.

[38] Rayleigh, Lord. "CXII. The problem of the whispering gallery." *The London, Edinburgh, and Dublin Philosophical Magazine and Journal of Science* 20.120 (1910): 1001-1004. https://doi.org/10.1080/14786441008636993

[39] D.L. Thomas, Dynamics of rotationally periodic structures, Int. J. Numer. Methods Eng. 14 (1979) 81–102. https://doi.org/10.1002/nme.1620140107.

[40] M. Kim, J. Moon, J. a. Wickert, Spatial Modulation of Repeated Vibration Modes in Rotationally Periodic Structures, J. Vib. Acoust. 122 (2000) 62. https://doi.org/10.1115/1.568443.

[41] E. Baruch, Y. Vered, H. Plat, I. Bucher, Active Detection of Small Imperfections in Structures With Cyclic Symmetry, J. Vib. Acoust. (2021). https://doi.org/10.1115/1.4049384.

[42] G.S. Happawana, A.K. Bajaj, O.D.I. Nwokah, A singular perturbation analysis of eigenvalue veering and modal sensitivity in perturbed linear periodic systems, J. Sound Vib. 160 (1993) 225–242. https://doi.org/10.1006/jsvi.1993.1019.

[43] Preumont, André, and Kazuto Seto. *Active control of structures*. John Wiley & Sons, 2008.

[44] S.-T. Wei, G. Research, A.C. Pierre, Localization Phenomena in Mistuned Assemblies with Cyclic Symmetry Part I: Free Vibrations, (1988). https://asmedigitalcollection.asme.org/vibrationacoustics/article-pdf/110/4/429/5435081/429_1.pdf (accessed April 6, 2020).

[45] I. Bucher, Estimating the ratio between travelling and standing vibration waves under non-stationary conditions, J. Sound Vib. 270 (2004) 341–359. https://doi.org/10.1016/S0022-460X(03)00539-X.

[46] I. Bucher, R. Gabai, H. Plat, A. Dolev, E. Setter, Experimental travelling waves identification in mechanical structures, Math. Mech. Solids. (2019). https://doi.org/10.1177/1081286517732825.

[47] J. Shi and B. Liu, “Optimum efficiency control of traveling-wave ultrasonic motor system,” *IEEE*

transactions on industrial electronics, vol. 58, no. 10, pp. 4822–4829, 2011.